Chapter 8
Nonlinear Effects

8.1 Introduction

Up to this point, we have limited our attention almost exclusively to *linear* phenomena; that is, to phenomena describable by equations in which the dependent variable occurs to no higher than the first power. The entire treatment of waves in Chap. 4, for instance, depended on the process of linearization, in which higher-order terms were regarded as small and were neglected. This procedure enabled us to consider only one Fourier component at a time, with the secure feeling that any nonsinusoidal wave can be handled simply by adding up the appropriate distribution of Fourier components. This works as long as the wave amplitude is small enough that the linear equations are valid.

Unfortunately, in many experiments waves are no longer describable by the linear theory by the time they are observed. Consider, for instance, the case of drift waves. Because they are unstable, drift waves would, according to linear theory, increase their amplitude exponentially. This period of growth is not normally observed—since one usually does not know when to start looking—but instead one observes the waves only after they have grown to a large, steady amplitude. The fact that the waves are no longer growing means that the linear theory is no longer valid, and some *nonlinear* effect is limiting the amplitude. Theoretical explanation of this elementary observation has proved to be a surprisingly difficult problem, since the observed amplitude at saturation is rather small.

A wave can undergo a number of changes when its amplitude gets large. It can change its shape—say, from a sine wave to a lopsided triangular waveform. This is the same as saying that Fourier components at other frequencies (or wave numbers) are generated. Ultimately, the wave can "break," like ocean waves on a beach, converting the wave energy into thermal energy of the particles. A large wave can

The original version of this chapter was revised. An erratum to this chapter can be found at https://doi.org/10.1007/978-3-319-22309-4_11

F.F. Chen, *Introduction to Plasma Physics and Controlled Fusion*,
DOI 10.1007/978-3-319-22309-4_8

trap particles in its potential troughs, thus changing the properties of the medium in which it propagates. We have already encountered this effect in discussing nonlinear Landau damping. If a plasma is so strongly excited that a continuous spectrum of frequencies is present, it is in a state of *turbulence*. This state must be described statistically, as in the case of ordinary fluid hydrodynamics. An important consequence of plasma turbulence is *anomalous resistivity*, in which electrons are slowed down by collisions with random electric field fluctuations, rather than with ions. This effect is used for ohmic heating of a plasma (Sect. 5.6.3) to temperatures so high that ordinary resistivity is insufficient.

Nonlinear phenomena can be grouped into three broad categories:

1. *Basically nonlinearizable problems*. Diffusion in a fully ionized gas, for instance, is intrinsically a nonlinear problem (Sect. 5.8) because the diffusion coefficient varies with density. In Sect. 6.1, we have seen that problems of hydromagnetic equilibrium are nonlinear. In Sect. 8.2, we shall give a further example—the important subject of plasma sheaths.
2. *Wave–particle interactions*. Particle trapping (Sect. 7.5) is an example of this and can lead to nonlinear damping. A classic example is the quasilinear effect, in which the equilibrium of the plasma is changed by the waves. Consider the case of a plasma with an electron beam (Fig. 8.1). Since the distribution function has a region where df_0/dv is positive, the system has inverse Landau damping, and plasma oscillations with v_ϕ in the positive-slope region are unstable (Eq. (7.67)). The resonant electrons are the first to be affected by wave–particle interactions, and their distribution function will be changed by the wave electric field. The waves are stabilized when $f_e(v)$ is flattened by the waves, as shown by the dashed line in Fig. 8.1, so that the new equilibrium distribution no longer has a positive slope. This is a typical quasilinear effect. Another example of wave–particle interactions, that of plasma wave echoes, will be given in Sect. 8.6.
3. *Wave–wave interactions*. Waves can interact with each other even in the fluid description, in which individual particle effects are neglected. A single wave can decay by first generating harmonics of its fundamental frequency. These harmonics can then interact with each other and with the primary wave to form other waves at the beat frequencies. The beat waves in turn can grow so large that they can interact and form many more beat frequencies, until the spectrum

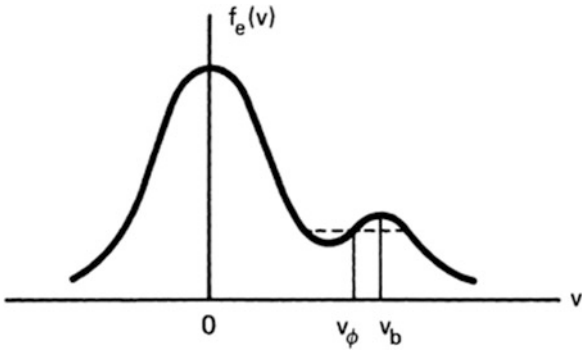

Fig. 8.1 A double-humped, unstable electron distribution

becomes continuous. It is interesting to discuss the direction of energy flow in a turbulent spectrum. In fluid dynamics, long-wavelength modes decay into short-wavelength modes, because the large eddies contain more energy and can decay only by splitting into small eddies, which are each less energetic. The smallest eddies then convert their kinetic motion into heat by viscous damping. In a plasma, usually the opposite occurs. Short-wavelength modes tend to coalesce into long-wavelength modes, which are less energetic. This is because the electric field energy $E^2/2$ is of order $k^2\phi^2/2$, so that if $e\phi$ is fixed (usually by KT_e), the small-k, long-λ modes have less energy. As a consequence, energy will be transferred to small k by instabilities at large k, and some mechanism must be found to dissipate the energy. No such problem exists at large k, where Landau damping can occur. For motions along B_0, nonlinear "modulational" instabilities could cause the energy at small k to be coupled to ions and to heat them. For motions perpendicular to B_0, the largest eddies will have wavelengths of the order of the plasma radius and could cause plasma loss to the walls by convection.

Although problems still remain to be solved in the linear theory of waves and instabilities, the mainstream of plasma research has turned to the much less well understood area of nonlinear phenomena. The examples in the following sections will give an idea of some of the effects that have been studied in theory and in experiment.

8.2 Sheaths

8.2.1 The Necessity for Sheaths

In all practical plasma devices, the plasma is contained in a vacuum chamber of finite size. What happens to the plasma at the wall? For simplicity, let us confine our attention to a one-dimensional model with no magnetic field (Fig. 8.2). Suppose there is no appreciable electric field inside the plasma; we can then let the potential ϕ be zero there. When ions and electrons hit the wall, they recombine and are lost. Since electrons have much higher thermal velocities than ions, they are lost faster

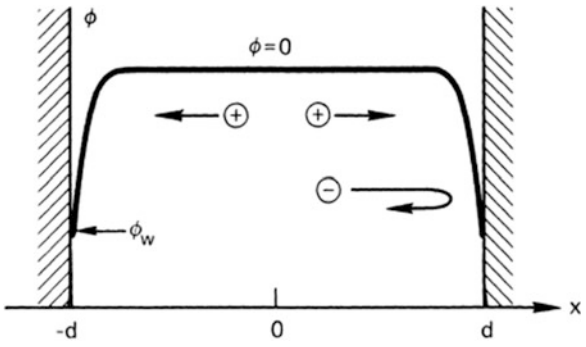

Fig. 8.2 The plasma potential ϕ forms sheaths near the walls so that electrons are reflected. The Coulomb barrier $e\phi_w$ adjusts itself so that equal numbers of ions and electrons reach the walls per second

and leave the plasma with a net positive charge. The plasma must then have a potential positive with respect to the wall; i.e., the wall potential ϕ_w is negative. This potential cannot be distributed over the entire plasma, since Debye shielding (Sect. 1.4) will confine the potential variation to a layer of the order of several Debye lengths in thickness. This layer, which must exist on all cold walls with which the plasma is in contact, is called a *sheath*. The function of a sheath is to form a potential barrier so that the more mobile species, usually electrons, is confined electrostatically. The height of the barrier adjusts itself so that the flux of electrons that have enough energy to go over the barrier to the wall is just equal to the flux of ions reaching the wall.

8.2.2 The Planar Sheath Equation

In Sect. 1.4, we linearized Poisson's equation to derive the Debye length. To examine the exact behavior of ϕ (x) in the sheath, we must treat the nonlinear problem; we shall find that there is not always a solution. Figure 8.3 shows the situation near one of the walls. At the plane $x = 0$, ions are imagined to enter the sheath region from the main plasma with a drift velocity u_0. This drift is needed to account for the loss of ions to the wall from the region in which they were created by ionization. For simplicity, we assume $T_i = 0$, so that all ions have the velocity u_0 at $x = 0$. We consider the steady state problem in a collisionless sheath region. The potential ϕ is assumed to decrease monotonically with x. Actually, ϕ could have spatial oscillations, and then there would be trapped particles in the steady state. This does not happen in practice because dissipative processes tend to destroy any such highly organized state.

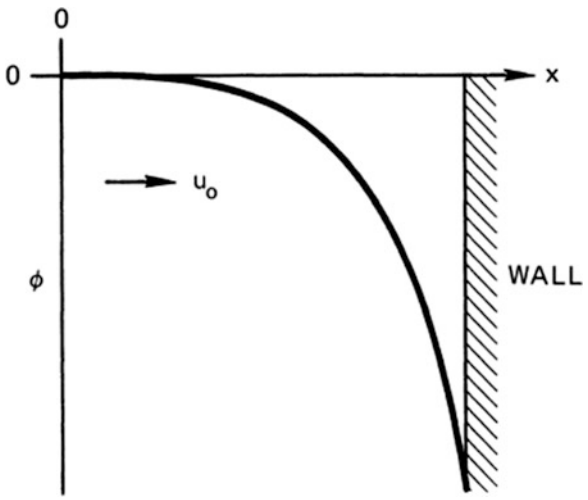

Fig. 8.3 The potential ϕ in a planar sheath. Cold ions are assumed to enter the sheath with a uniform velocity u_0

If $u(x)$ is the ion velocity in the sheath, conservation of energy requires

$$\frac{1}{2}\,Mu^2 = \frac{1}{2}Mu_0^2 - e\phi(x) \tag{8.1}$$

$$u = \left(u_0^2 - \frac{2e\phi}{M}\right)^{1/2} \tag{8.2}$$

The ion equation of continuity then gives the ion density n_i in terms of the density n_0 in the main plasma:

$$n_0 u_0 = n_i(x)\;\; u(x) \tag{8.3}$$

$$n_i(x) = n_0\left(1 - \frac{2e\phi}{Mu_0^2}\right)^{-1/2} \tag{8.4}$$

In steady state, the electrons will follow the Boltzmann relation closely:

$$n_e(x) = n_0 \exp(e\phi/KT_e) \tag{8.5}$$

Poisson's equation is then

$$\varepsilon_0 \frac{d^2\phi}{dx^2} = e(n_e - n_i) = en_0\left[\exp\left(\frac{e\phi}{KT_e}\right) - \left(1 - \frac{2e\phi}{Mu_0^2}\right)^{-1/2}\right] \tag{8.6}$$

The structure of this equation can be seen more clearly if we simplify it with the following changes in notation:

$$\chi \equiv -\frac{e\phi}{KT_e}, \qquad \xi \equiv \frac{x}{\lambda_D} = x\left(\frac{n_0 e^2}{\varepsilon_0 KT_e}\right)^{1/2} \qquad \mathcal{M} \equiv \frac{u_0}{(KT_e/M)^{1/2}} \tag{8.7}$$

Then Eq. (8.6) becomes

$$\chi'' = \left(1 + \frac{2\chi}{\mathcal{M}^2}\right)^{-1/2} - e^{-\chi} \tag{8.8}$$

where the prime denotes $d/d\xi$. This is the nonlinear equation of a plane sheath, and it has an acceptable solution only if $\mathcal{M}$ is large enough. The reason for the symbol $\mathcal{M}$ will become apparent in the following section on shock waves.

8.2.3 The Bohm Sheath Criterion

Equation (8.8) can be integrated once by multiplying both sides by χ':

$$\int_0^\xi \chi'\chi'' d\xi_1 = \int_0^\xi \left(1+\frac{2\chi}{\mathcal{M}^2}\right)^{-1/2} \chi' d\xi_1 - \int_0^\xi e^{-\chi}\chi' d\xi_1 \tag{8.9}$$

where ξ_1 is a dummy variable. Since $\chi = 0$ at $\xi = 0$, the integrations easily yield

$$\frac{1}{2}\left(\chi'^2 - \chi_0'^2\right) = \mathcal{M}^2\left[\left(1+\frac{2\chi}{\mathcal{M}^2}\right)^{1/2} - 1\right] + e^{-\chi} - 1. \tag{8.10}$$

If $\mathbf{E} = 0$ in the plasma, we must set $\chi_0' = 0$ at $\xi = 0$. A second integration to find χ would have to be done numerically; but whatever the answer is, the right-hand side of Eq. (8.10) must be positive for all χ. In particular, for $\chi \ll 1$, we can expand the right-hand terms in Taylor series:

$$\begin{gathered}\mathcal{M}^2\left[1+\frac{\chi}{\mathcal{M}^2} - \frac{1}{2}\frac{\chi^2}{\mathcal{M}^4} + \cdots - 1\right] + 1 - \chi + \frac{1}{2}\chi^2 + \cdots - 1 > 0 \\ \frac{1}{2}\chi^2\left(-\frac{1}{\mathcal{M}^2}+1\right) > 0 \\ \mathcal{M}^2 > 1 \qquad \text{or} \qquad u_0 > (KT_e/M)^{1/2}\end{gathered} \tag{8.11}$$

This inequality is known as the *Bohm sheath criterion*. It says that ions must enter the sheath region with a velocity greater than the acoustic velocity v_s. To give the ions this directed velocity u_0, there must be a finite electric field in the plasma. Our assumption that $\chi' = 0$ at $\xi = 0$ is therefore only an approximate one, made possible by the fact that the scale of the sheath region is usually much smaller than the scale of the main plasma region in which the ions are accelerated. The value of u_0 is somewhat arbitrary, depending on where we choose to put the boundary $x = 0$ between the plasma and the sheath. Of course, the ion flux n_0u_0 is fixed by the ion production rate, so if u_0 is varied, the value of n_0 at $x = 0$ will vary inversely with u_0. If the ions have finite temperature, the critical drift velocity u_0 will be somewhat lower.

The physical reason for the Bohm criterion is easily seen from a plot of the ion and electron densities vs. χ (Fig. 8.4). The electron density n_e falls exponentially with χ according to the Boltzmann relation. The ion density also falls, since the ions are accelerated by the sheath potential. If the ions start with a large energy, $n_i(\chi)$ falls slowly, since the sheath field causes a relatively minor change in the ions' velocity. If the ions start with a small energy, $n_i(\chi)$ falls fast, and can go below the n_e curve. In that case, $n_e - n_i$ is positive near $\chi = 0$; and Eq. (8.6) tells us that $\phi(x)$ must curve upward, in contradiction to the requirement that the sheath must repel

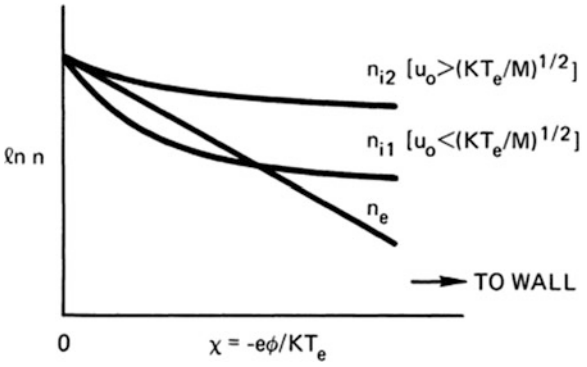

Fig. 8.4 Variation of ion and electron density (logarithmic scale) with normalized potential χ in a sheath. The ion density is drawn for two cases: u_0 greater than and u_0 less than the critical velocity

electrons. In order for this not to happen, the slope of $n_i(\chi)$ at $\chi = 0$ must be smaller (in absolute value) than that of $n_e(\chi)$; this condition is identical with the condition $\mathcal{M}^2 > 1$.

8.2.4 The Child–Langmuir Law

Since $n_e(\chi)$ falls exponentially with χ, the electron density can be neglected in the region of large χ next to the wall (or any negative electrode). Poisson's equation is then approximately

$$\chi'' \approx \left(1 + \frac{2\chi}{\mathcal{M}^2}\right)^{-1/2} \approx \frac{\mathcal{M}}{(2\chi)^{1/2}} \tag{8.12}$$

Multiplying by χ' and integrating from $\xi_1 = \xi_s$ to $\xi_1 = \xi$, we have

$$\frac{1}{2}\left(\chi'^2 - \chi_s'^2\right) = \sqrt{2}\mathcal{M}\left(\chi^{1/2} - \chi_s^{1/2}\right) \tag{8.13}$$

where ξ_s is the place where we started neglecting n_e. We can redefine the zero of χ so that $\chi_s = 0$ at $\xi = \xi_s$. We shall also neglect χ_s', since the slope of the potential curve can be expected to be much steeper in the $n_e = 0$ region than in the finite-n_e region. Then Eq. (8.13) becomes

$$\begin{aligned} \chi'^2 &= 2^{3/2}\mathcal{M}\chi^{1/2} \\ \chi' &= 2^{3/4}\mathcal{M}^{1/2}\chi^{1/4} \end{aligned} \tag{8.14}$$

or

$$d\chi/\chi^{1/4} = 2^{3/4}\mathcal{M}^{1/2}d\xi. \tag{8.15}$$

Integrating from $\xi = \xi_s$ to $\xi = \xi_s + d/\lambda_D = \xi_{wall}$, we have

$$\frac{4}{3}\chi_w^{3/4} = 2^{3/4}\mathcal{M}^{1/2} d/\lambda_D \tag{8.16}$$

or

$$\mathcal{M} = \frac{4\sqrt{2}}{9}\frac{\chi_w^{3/2}}{d^2}\lambda_D^2 \tag{8.17}$$

Changing back to the variables u_0 and ϕ, and noting that the ion current into the wall is $J = en_0u_0$, we then find

$$J = \frac{4}{9}\left(\frac{2e}{M}\right)^{1/2}\frac{\varepsilon_0|\phi_w|^{3/2}}{d^2} \tag{8.18}$$

This is just the well-known Child–Langmuir law of space-charge-limited current in a plane diode.

The potential variation in a plasma–wall system can be divided into three parts. Nearest the wall is an electron-free region whose thickness d is given by Eq. (8.18). Here J is determined by the ion production rate, and ϕ_w is determined by the equality of electron and ion fluxes. Next comes a region in which n_e is appreciable; as shown in Sect. 1.4, this region has the scale of the Debye length. Finally, there is a region with much larger scale length, the "presheath," in which the ions are accelerated to the required velocity u_0 by a potential drop $|\phi| \geq \frac{1}{2}KT_e/e$. Depending on the experiment, the scale of the presheath may be set by the plasma radius, the collision mean free path, or the ionization mechanism. The potential distribution, of course, varies smoothly; the division into three regions is made only for convenience and is made possible by the disparity in scale lengths. In the early days of gas discharges, sheaths could be observed as dark layers where no electrons were present to excite atoms to emission. Subsequently, the potential variation has been measured by the electrostatic deflection of a thin electron beam shot parallel to a wall.

Recent theories of discharges in finite cylinders show that the sheaths on the endplates play an essential rôle in moving plasma created at the radial edge towards the axis, so that the final density profile is peaked at the center. It has also been shown that the density profile in such a plasma, including the presheath, tends to fall into a universal shape independent of pressure and discharge diameter.

8.2.5 *Electrostatic Probes*

The sheath criterion, Eq. (8.11), can be used to estimate the flux of ions to a negatively biased probe in a plasma. If the probe has a surface area A, and if the ions entering the sheath have a drift velocity $u_0 \geq (KT_e/M)^{1/2}$, then the ion current collected is

$$I = n_s eA(KT_e/M)^{1/2} \tag{8.19}$$

The electron current can be neglected if the probe is sufficiently negative (several times KT_e) relative to the plasma to repel all but the tail of the Maxwellian electron distribution. The density n_s is the plasma density at the edge of the sheath. Let us define the sheath edge to be the place where u_0 is exactly $(KT_e/M)^{1/2}$. To accelerate ions to this velocity requires a presheath potential $|\phi| \geq \frac{1}{2}KT_e/e$, so that the sheath edge has a potential

$$\phi_s \simeq -\frac{1}{2}KT_e/e \tag{8.20}$$

relative to the body of the plasma. If the electrons are Maxwellian, this determines n_s:

$$n_s = n_0 e^{e\phi_s/kT_e} = n_0 e^{-1/2} = 0.61 n_0 \tag{8.21}$$

For our purposes it is accurate enough to replace 0.61 with a round number like 1/2; thus, the "saturation ion current" to a negative probe is approximately

$$I_B = \frac{1}{2} n_0 eA(KT_e/M)^{1/2} \tag{8.22}$$

I_B, sometimes called the "Bohm current," gives the plasma density easily, once the temperature is known.

If the Debye length λ_D, and hence the sheath thickness, is very small compared to the probe dimensions, the area of the sheath edge is effectively the same as the area A of the probe surface, regardless of its shape. At low densities, however, λ_D can become large, so that some ions entering the sheath can orbit the probe and miss it. Calculations of orbits for various probe shapes were first made by I. Langmuir and L. Tonks—hence the name "Langmuir probe" ascribed to this method of measurement. Though tedious, these calculations can give accurate determinations of plasma density because an arbitrary definition of sheath edge does not have to be made. By varying the probe voltage, the electron distribution is sampled, and the current–voltage curve of a Langmuir probe can also yield the electron temperature, if the electrons are Maxwellian, or their velocity distribution if they are not. The Langmuir probe is the first plasma diagnostic and is still the simplest and the most localized measurement device. Material electrodes can be inserted only in low-density, cool plasmas. Nonetheless, these include most non-fusion laboratory plasmas, and an extensive literature exists on probe theory. The problem with using a large probe, to which Eq. (8.22) applies, is that it collects from an ill-defined sheath edge that surrounds it, and it may also disturb the plasma. Thin cylindrical probes with radii $\leq \lambda_D$ are more commonly used.

Problems

8.1 A probe whose collecting surface is a square tantalum foil 2×2 mm in area is found to give a saturation ion current of 100 μA in a singly ionized argon plasma (atomic weight = 40). If $KT_e = 2$ eV, what is the approximate plasma density? (Hint: Both sides of the probe collect ions!)

8.2 A solar satellite consisting of 10 km^2 of photovoltaic panels is placed in synchronous orbit around the earth. It is immersed in a 1-eV atomic hydrogen plasma at density 10^6 m^{-3}. During solar storms the satellite is bombarded by energetic electrons, which charge it to a potential of -2 kV. Calculate the flux of energetic ions bombarding each m^2 of the panels.

8.3 The sheath criterion of Eq. (8.11) was derived for a cold-ion plasma. Suppose the ion distribution had a thermal spread in velocity around an average drift speed u_0. Without mathematics, indicate whether you would expect the value of u_0 to be above or below the Bohm value, and explain why.

8.4 An ion velocity analyzer consists of a stainless steel cylinder 5 mm in diameter with one end covered with a fine tungsten mesh grid (grid 1). Behind this, inside the cylinder, are a series of insulated, parallel grids. Grid 1 is at "floating" potential—it is not electrically connected. Grid 2 is biased negative to repel all electrons coming through grid 1, but it transmits ions. Grid 3 is the analyzer grid, biased so as to decelerate ions accelerated by grid 2. Those ions able to pass through grid 3 are all collected by a collector plate. Grid 4 is a suppressor grid that turns back secondary electrons emitted by the collector. If the plasma density is too high, a space charge problem occurs near grid 3 because the ion density is so large that a potential hill forms in front of grid 3 and repels ions which would otherwise reach grid 3. Using the Child–Langmuir law, estimate the maximum meaningful He^+ current that can be measured on a 4-mm-diam collector if grids 2 and 3 are separated by 1 mm and 100 V.

8.3 Ion Acoustic Shock Waves

When a jet travels faster than sound, it creates a shock wave. This is a basically nonlinear phenomenon, since there is no period when the wave is small and growing. The jet is faster than the speed of waves in air, so the undisturbed medium cannot be "warned" by precursor signals before the large shock wave hits it. In hydrodynamic shock waves, collisions are dominant. Shock waves also exist in plasmas, even when there are no collisions. A magnetic shock, the "bow shock," is generated by the earth as it plows through the interplanetary plasma while dragging along a dipole magnetic field. We shall discuss a simpler example: a collisionless, one-dimensional shock wave which develops from a large-amplitude ion wave.

8.3.1 The Sagdeev Potential

Figure 8.5 shows the idealized potential profile of an ion acoustic shock wave. The reason for this shape will be given presently. The wave is traveling to the left with a velocity u_0. If we go to the frame moving with the wave, the function $\phi(x)$ will be constant in time, and we will see a stream of plasma impinging on the wave from the left with a velocity u_0. For simplicity, let T_i be zero, so that all the ions are incident with the same velocity u_0, and let the electrons be Maxwellian. Since the shock moves much more slowly than the electron thermal speed, the shift in the center velocity of the Maxwellian can be neglected. The velocity of the ions in the shock wave is, from energy conservation,

$$u = \left(u_0^2 - \frac{2e\phi}{M}\right)^{1/2} \tag{8.23}$$

If n_0 is the density of the undisturbed plasma, the ion density in the shock is

$$n_i = \frac{n_0 u_0}{u} = n_0\left(1 - \frac{2e\phi}{Mu_0^2}\right)^{-1/2} \tag{8.24}$$

The electron density is given by the Boltzmann relation. Poisson's equation then gives

$$\varepsilon_0 \frac{d^2\phi}{dx^2} = e(n_e - n_i) = en_0\left[\exp\left(\frac{e\phi}{KT_e}\right) - \left(1 - \frac{2e\phi}{Mu_0^2}\right)^{-1/2}\right] \tag{8.25}$$

This is, of course, the same equation (Eq. (8.6)) as we had for a sheath. A shock wave is no more than a sheath moving through a plasma. We now introduce the dimensionless variables

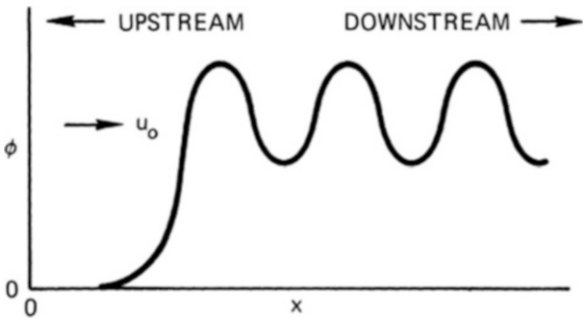

Fig. 8.5 Typical potential distribution in an ion acoustic shock wave. The wave moves to the left, so that in the wave frame ions stream into the wave from the left with velocity u_0

$$\chi \equiv +\frac{e\phi}{KT_e} \qquad \xi \equiv \frac{x}{\lambda_D} \qquad \mathcal{M} \equiv \frac{u_0}{(KT_e/M)^{1/2}} \tag{8.26}$$

Note that we have changed the sign in the definition of χ so as to keep χ positive in this problem as well as in the sheath problem. The quantity $\mathcal{M}$ is called the *Mach number* of the shock. Equation (8.25) can now be written

$$\frac{d^2\chi}{d\xi^2} = e^{\chi} - \left(1 - \frac{2\chi}{\mathcal{M}^2}\right)^{-1/2} \equiv -\frac{dV(\chi)}{d\chi} \tag{8.27}$$

which differs from the sheath equation (8.8) only because of the change in sign of χ.

The behavior of the solution of Eq. (8.27) was made clear by R. Z. Sagdeev, who used an analogy to an oscillator in a potential well. The displacement x of an oscillator subjected to a force $-m \cdot dV(x)/dx$ is given by

$$d^2x/dt^2 = -dV/dx \tag{8.28}$$

If the right-hand side of Eq. (8.27) is defined as $-dV/d\chi$, the equation is the same as that of an oscillator, with the potential χ playing the role of x, and $d/d\xi$ replacing d/dt. The quasipotential $V(\chi)$ is sometimes called the Sagdeev potential. The function $V(\chi)$ can be found from Eq. (8.27) by integration with the boundary condition $V(\chi) = 0$ at $\chi = 0$:

$$V(\chi) = 1 - e^{\chi} + \mathcal{M}^2\left[1 - \left(1 - \frac{2\chi}{\mathcal{M}^2}\right)^{1/2}\right] \tag{8.29}$$

For $\mathcal{M}$ lying in a certain range, this function has the shape shown in Fig. 8.6. If this were a real well, a particle entering from the left will go to the right-hand side of the

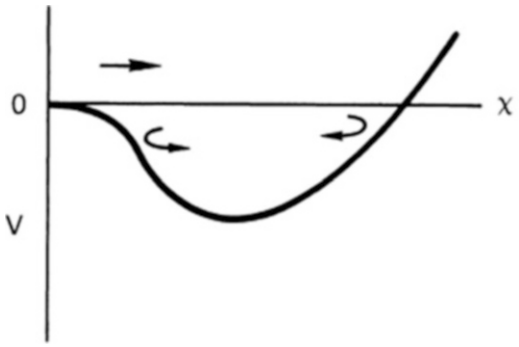

Fig. 8.6 The Sagdeev potential $V(\chi)$. The *upper arrow* is the trajectory of a quasiparticle describing a soliton: it is reflected at the right and returns. The *lower arrows* show the motion of a quasiparticle that has lost energy and is trapped in the potential well. The bouncing back and forth describes the oscillations behind a shock front

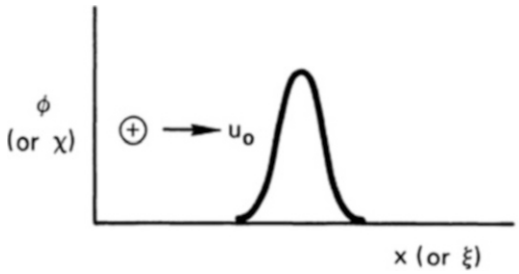

Fig. 8.7 The potential in a soliton moving to the left

well ($x > 0$), reflect, and return to $x = 0$, making a single transit. Similarly, a quasiparticle in our analogy will make a single excursion to positive χ and return to $\chi = 0$, as shown in Fig. 8.7. Such a pulse is called a *soliton*; it is a potential and density disturbance propagating to the left in Fig. 8.7 with velocity u_0.

Now, if a particle suffers a loss of energy while in the well, it will never return to $x = 0$ but will oscillate (in time) about some positive value of x. Similarly, a little dissipation will make the potential of a shock wave oscillate (in space) about some positive value of ϕ. This is exactly the behavior depicted in Fig. 8.5. Actually, dissipation is not needed for this; reflection of ions from the shock front has the same effect. To understand this, imagine that the ions have a small thermal spread in energy and that the height $e\phi$ of the wave front is just large enough to reflect some of the ions back to the left, while the rest go over the potential hill to the right. The reflected ions cause an increase in ion density in the upstream region to the left of the shock front (Fig. 8.5). This means that the quantity

$$\chi' = \frac{1}{n_0}\int_0^{\xi} (n_e - n_i)d\xi_1 \tag{8.30}$$

is decreased. Since χ' is the analog of dx/dt in the oscillator problem, our virtual oscillator has lost velocity and is trapped in the potential well of Fig. 8.6.

8.3.2 *The Critical Mach Numbers*

Solutions of either the soliton type or the wave-train type exist only for a range of $\mathcal{M}$. A lower limit for $\mathcal{M}$ is given by the condition that $V(\chi)$ be a potential well, rather than a hill. Expanding Eq. (8.29) for $\chi \ll 1$ yields

$$\tfrac{1}{2}\chi^2 - \left(\chi^2/2\mathcal{M}^2\right) > 0 \qquad \mathcal{M}^2 > 1 \tag{8.31}$$

This is exactly the same, both physically and mathematically, as the Bohm criterion for the existence of a sheath (Eq. (8.11)).

An upper limit to $\mathcal{M}$ is imposed by the condition that the function $V(\chi)$ of Fig. 8.6 must cross the χ axis for $\chi > 0$; otherwise, the virtual particle will not be reflected, and the potential will rise indefinitely. From Eq. (8.29), we require

$$e^{\chi} - 1 < \mathcal{M}^2 \left[1 - \left(1 - \frac{2\chi}{\mathcal{M}^2} \right)^{1/2} \right] \tag{8.32}$$

for some $\chi > 0$. If the lower critical Mach number is surpassed ($\mathcal{M} > 1$), the left-hand side, representing the integral of the electron density from zero to χ, is initially larger than the right-hand side, representing the integral of the ion density. As χ increases, the right-hand side can catch up with the left-hand side if $\mathcal{M}^2$ is not too large. However, because of the square root, the largest value χ can have is $\mathcal{M}^2/2$. This is because $e\phi$ cannot exceed $\frac{1}{2}Mu_0^2$; otherwise, ions would be excluded from the plasma in the downstream region. Inserting the largest value of χ into Eq. (8.32), we have

$$\exp\left(\mathcal{M}^2/2\right) - 1 < \mathcal{M}^2 \qquad \text{or} \qquad \mathcal{M} < 1.6 \tag{8.33}$$

This is the upper critical Mach number. Shock waves in a cold-ion plasma therefore exist only for $1 < \mathrm{M} < 1.6$.

As in the case of sheaths, the physical situation is best explained by a diagram of n_i and n_e vs. χ (Fig. 8.8). This diagram differs from Fig. 8.4 because of the change of sign of ϕ. Since the ions are now decelerated rather than accelerated, n_i will approach infinity at $\chi = \mathcal{M}^2/2$. The lower critical Mach number ensures that the n_i curve lies below the n_e curve at small χ, so that the potential $\phi(x)$ starts off with the right sign for its curvature. When the curve n_{i1} crosses the n_e curve, the soliton $\phi(x)$ (Fig. 8.7) has an inflection point. Finally, when χ is large enough that the areas under the n_i and n_e curves are equal, the soliton reaches a peak, and the n_{i1} and n_e

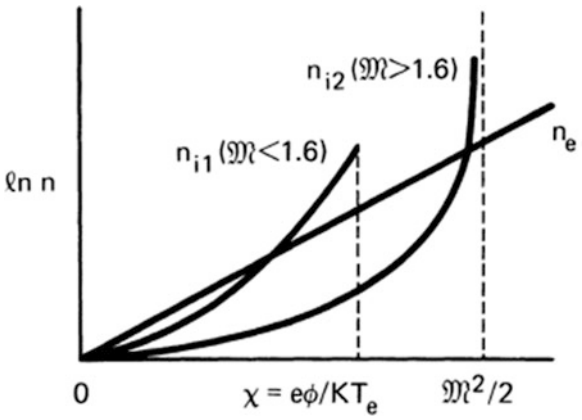

Fig. 8.8 Variation of ion and electron density (logarithmic scale) with normalized potential χ in a soliton. The ion density is drawn for two cases: Mach number greater than and less than 1.6

curves are retraced as χ goes back to zero. The equality of the areas ensures that the net charge in the soliton is zero; therefore, there is no electric field outside. If $\mathcal{M}$ is larger than 1.6, we have the curve n_{i2}, in which the area under the curve is too small even when χ has reached its maximum value of $\mathcal{M}^2/2$.

8.3.3 *Wave Steepening*

If one propagates an ion wave in a cold-ion plasma, it will have the phase velocity given by Eq. (4.42), corresponding to $\mathcal{M} = 1$. How, then, can one create shocks with $\mathcal{M} > 1$? One must remember that Eq. (4.42) was a linear result valid only at small amplitudes. As the amplitude is increased, an ion wave speeds up and also changes from a sine wave to a sawtooth shape with a steep leading edge (Fig. 8.9). The reason is that the wave electric field has accelerated the ions. In Fig. 8.9, ions at the peak of the potential distribution have a larger velocity in the direction of v_ϕ than those at the trough, since they have just experienced a period of acceleration as the wave passed by. In linear theory, this difference in velocity is taken into account, but not the displacement resulting from it. In nonlinear theory, it is easy to see that the ions at the peak are shifted to the right, while those at the trough are shifted to the left, thus steepening the wave shape. Since the density perturbation is in phase with the potential, more ions are accelerated to the right than to the left, and the wave causes a net mass flow in the direction of propagation. This causes the wave velocity to exceed the acoustic speed in the undisturbed plasma, so that $\mathcal{M}$ is larger than unity.

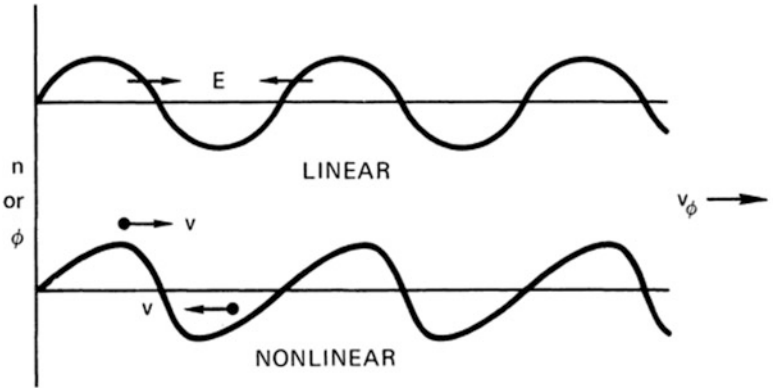

Fig. 8.9 A large-amplitude ion wave steepens so that the leading edge has a larger slope than the trailing edge

8.3.4 Experimental Observations

Ion acoustic shock waves of the form shown in Fig. 8.5 have been generated by R. J. Taylor, D. R. Baker, and H. Ikezi. To do this, a new plasma source, the DP (double-plasma) device, was invented. Figure 8.10 shows schematically how it works. Identical plasmas are created in two electrically isolated chambers by discharges between filaments F and the walls W. The plasmas are separated by the negatively biased grid G, which repels electrons and forms an ion sheath on both sides. A voltage pulse, usually in the form of a ramp, is applied between the two chambers. This causes the ions in one chamber to stream into the other, exciting a large-amplitude plane wave. The wave is detected by a movable probe or particle velocity analyzer P. Figure 8.11 shows measurements of the density fluctuation in the shock wave as a function of time and probe position. It is seen that the wavefront steepens and then turns into a shock wave of the classic shape. The damping of the oscillations is due to collisions.

Problem

8.5 Calculate the maximum possible velocity of an ion acoustic shock wave in an experiment such as that shown in Fig. 8.10, where $T_e = 1.5$ eV, $T_i = 0.2$ eV, and the gas is argon. What is the maximum possible shock wave amplitude in volts?

8.3.5 Double Layers

A phenomenon related to sheaths and ion acoustic shocks is that of the double layer. This is a localized potential jump, believed to occur naturally in the ionosphere,

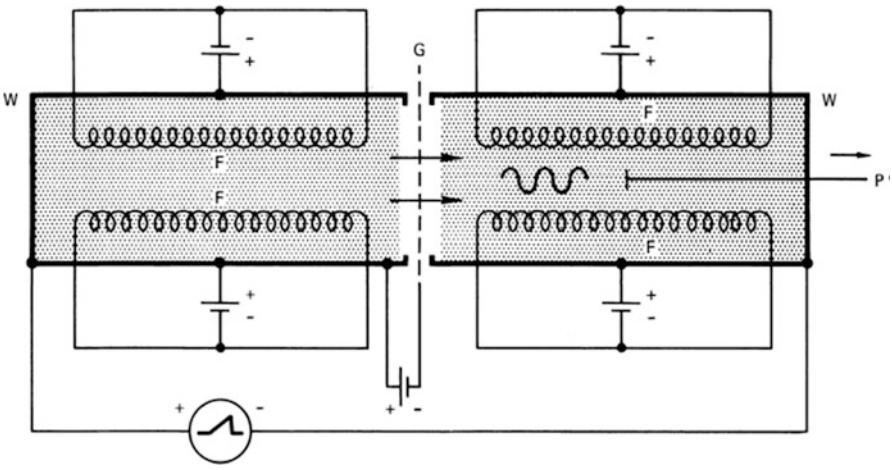

Fig. 8.10 Schematic of a DP machine in which ion acoustic shock waves were produced and detected. [*Cf.* R. J. Taylor, D. R. Baker, and H. Ikezi, *Phys. Rev. Lett.* **24**, 206 (1970).]

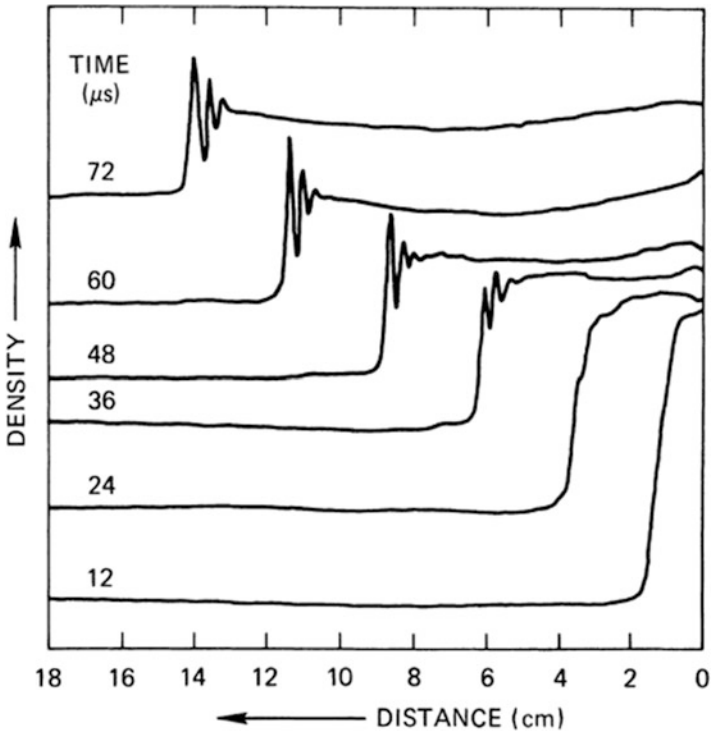

Fig. 8.11 Measurements of the density distribution in a shock wave at various times, showing how the characteristic shape of Fig. 8.5 develops. [From Taylor *et al.*, *loc cit.*]

which neither propagates nor is attached to a boundary. The name comes from the successive layers of net positive and net negative charge that are necessary to create a step in $\phi(x)$. Such a step can remain stationary in space only if there is a plasma flow that Doppler-shifts a shock front down to zero velocity in the lab frame, or if the distribution functions of the transmitted and reflected electrons and ions on each side of the discontinuity are specially tailored so as to make this possible. Double layers have been created in the laboratory in "triple-plasma" devices, which are similar to the DP machine shown in Fig. 8.10, but with a third experimental chamber (without filaments) inserted between the two source chambers. By adjusting the relative potentials of the three chambers, which are isolated by grids, streams of ions or electrons can be spilled into the center chamber to form a double layer there. In natural situations double layers are likely to arise where there are gradients in the magnetic field **B**, not where **B** is zero or uniform as in laboratory simulations. In that case, the $\mu\nabla B$ force (Eq. (2.38)) can play a large role in localizing a double layer away from all boundaries. Indeed, the thermal barrier in tandem mirror reactors is an example of a double layer with strong magnetic trapping. In Sect. 8.11 we shall see that a double layer can arise in "mid-air" when a dense plasma is injected into a diverging magnetic field. Ions accelerated by the potential drop in the double layer can be used to push a spacecraft.

8.4 The Ponderomotive Force

Light waves exert a radiation pressure which is usually very weak and hard to detect. Even the esoteric example of comet tails, formed by the pressure of sunlight, is tainted by the added effect of particles streaming from the sun. When high-powered microwaves or laser beams are used to heat or confine plasmas, however, the radiation pressure can reach several hundred thousand atmospheres! When applied to a plasma, this force is coupled to the particles in a somewhat subtle way and is called the *ponderomotive force*. Many nonlinear phenomena have a simple explanation in terms of the ponderomotive force.

The easiest way to derive this nonlinear force is to consider the motion of an electron in the oscillating **E** and **B** fields of a wave. We neglect dc $\mathbf{E_0}$ and $\mathbf{B_0}$ fields. The electron equation of motion is

$$m\frac{d\mathbf{v}}{dt} = -e[\mathbf{E}(\mathbf{r}) + \mathbf{v} \times \mathbf{B}(\mathbf{r})] \tag{8.34}$$

This equation is exact if **E** and **B** are evaluated at the instantaneous position of the electron. The nonlinearity comes partly from the $\mathbf{v} \times \mathbf{B}$ term, which is second order because both **v** and **B** vanish in the equilibrium, so that the term is no larger than $\mathbf{v}_1 \times \mathbf{B}_1$, where $\mathbf{v}_1$ and $\mathbf{B}_1$ are the linear-theory values. The other part of the nonlinearity, as we shall see, comes from evaluating **E** at the actual position of the particle rather than its initial position. Assume a wave electric field of the form

$$\mathbf{E} = \mathbf{E}_s(\mathbf{r}) \cos \omega t \tag{8.35}$$

where $\mathbf{E}_s(\mathbf{r})$ contains the spatial dependence. In first order, we may neglect the $\mathbf{v} \times \mathbf{B}$ term in Eq. (8.34) and evaluate **E** at the initial position $\mathbf{r}_0$. We have

$$m d\mathbf{v}_1/dt = -e\mathbf{E}(\mathbf{r}_0) \tag{8.36}$$

$$\mathbf{v}_1 = -(e/m\omega)\mathbf{E}_s \sin \omega t = d\mathbf{r}_1/dt \tag{8.37}$$

$$\delta\mathbf{r}_1 = \left(e/m\omega^2\right)\mathbf{E}_s \cos \omega t \tag{8.38}$$

It is important to note that in a nonlinear calculation, we cannot write $e^{i\omega t}$ and take its real part later. Instead, we write its real part explicitly as cos ωt. This is because products of oscillating factors appear in nonlinear theory, and the operations of multiplying and taking the real part do not commute.

Going to second order, we expand $\mathbf{E}(\mathbf{r})$ about $\mathbf{r_0}$:

$$\mathbf{E}(\mathbf{r}) = \mathbf{E}(\mathbf{r}_0) + (\delta\mathbf{r}_1 \cdot \nabla)\mathbf{E}|_{r=r_0} + \cdots \tag{8.39}$$

We must now add the term $\mathbf{v}_1 \times \mathbf{B}_1$, where $\mathbf{B}_1$ is given by Maxwell's equation:

$$\begin{aligned} \nabla \times \mathbf{E} &= -\partial \mathbf{B}/\partial t \\ \mathbf{B}_1 &= -(1/\omega)\nabla \times \mathbf{E}_s|_{r=r_0} \sin \omega t \end{aligned} \tag{8.40}$$

The second-order part of Eq. (8.34) is then

$$m d\mathbf{v}_2/dt = -e[(\delta \mathbf{r}_1 \cdot \nabla)\mathbf{E} + \mathbf{v}_1 \times \mathbf{B}_1] \tag{8.41}$$

Inserting Eqs. (8.37), (8.38), and (8.40) into (8.41) and averaging over time, we have

$$m\left\langle \frac{d\mathbf{v}_2}{dt} \right\rangle = -\frac{e^2}{m\omega^2}\frac{1}{2}[(\mathbf{E}_s \cdot \nabla)\mathbf{E}_s + \mathbf{E}_s \times (\nabla \times \mathbf{E}_s)] = \mathbf{f}_{\mathrm{NL}} \tag{8.42}$$

Here we used $\langle \sin^2 \omega t \rangle = \langle \cos^2 \omega t \rangle = ½$. The double cross product can be written as the sum of two terms, one of which cancels the $(\mathbf{E}_s \cdot \nabla)\mathbf{E}_s$ term. What remains is

$$\mathbf{f}_{\mathrm{NL}} = -\frac{1}{4}\frac{e^2}{m\omega^2}\nabla E_s^2 \tag{8.43}$$

This is the effective nonlinear force on a single electron. The force per m^3 is $\mathbf{f}_{\mathrm{NL}}$ times the electron density n_0, which can be written in terms of ω_p^2. Since $E_s^2 = 2\langle E^2 \rangle$, we finally have for the ponderomotive force the formula

$$\mathbf{F}_{\mathrm{NL}} = -\frac{\omega_p^2}{\omega^2}\nabla \frac{\langle \varepsilon_0 E^2 \rangle}{2} \tag{8.44}$$

If the wave is electromagnetic, the second term in Eq. (8.42) is dominant, and the physical mechanism for $\mathbf{F}_{\mathrm{NL}}$ is as follows. Electrons oscillate in the direction of $\mathbf{E}$, but the wave magnetic field distorts their orbits. That is, the Lorentz force $-e\mathbf{v} \times \mathbf{B}$ pushes the electrons in the direction of $\mathbf{k}$ (since $\mathbf{v}$ is in the direction of $\mathbf{E}$, and $\mathbf{E} \times \mathbf{B}$ is in the direction of $\mathbf{k}$). The phases of $\mathbf{v}$ and $\mathbf{B}$ are such that the motion does not average to zero over an oscillation, but there is a secular drift along $\mathbf{k}$. If the wave has uniform amplitude, no force is needed to maintain this drift; but if the wave amplitude varies, the electrons will pile up in regions of small amplitude, and a force is needed to overcome the space charge. This is why the effective force $\mathbf{F}_{\mathrm{NL}}$ is proportional to the *gradient* of $\langle \mathrm{E}^2 \rangle$. Since the drift for each electron is the same, $\mathbf{F}_{\mathrm{NL}}$ is proportional to the density—hence the factor ω_p^2/ω^2 in Eq. (8.44).

If the wave is electrostatic, the first term in Eq. (8.42) is dominant. Then the physical mechanism is simply that an electron oscillating along $\mathbf{k} \parallel \mathbf{E}$ moves farther in the half-cycle when it is moving from a strong-field region to a weak-field region than vice versa, so there is a net drift.

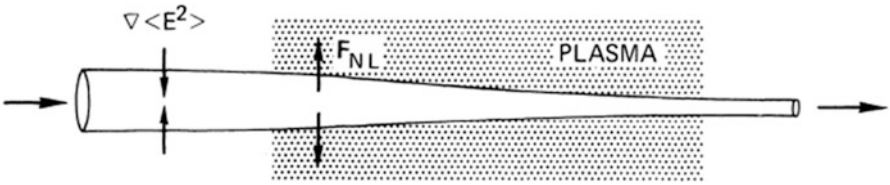

Fig. 8.12 Self-focusing of a laser beam is caused by the ponderomotive force

Although $\mathbf{F}_{\mathrm{NL}}$ acts mainly on the electrons, the force is ultimately transmitted to the ions, since it is a low-frequency or dc effect. When electrons are bunched by $\mathbf{F}_{\mathrm{NL}}$, a charge-separation field $\mathbf{E}_{\mathrm{cs}}$ is created. The total force felt by the electrons is

$$\mathbf{F}_e = -e\mathbf{E}_{\mathrm{cs}} + \mathbf{F}_{\mathrm{NL}} \tag{8.45}$$

Since the ponderomotive force on the ions is smaller by $\Omega_p^2/\omega_p^2 = m/M$, the force on the ion fluid is approximately

$$\mathbf{F}_i = e\mathbf{E}_{\mathrm{cs}} \tag{8.46}$$

Summing the last two equations, we find that the force on the plasma is $\mathbf{F}_{\mathrm{NL}}$.

A direct effect of $\mathbf{F}_{\mathrm{NL}}$ is the self-focusing of laser light in a plasma. In Fig. 8.12 we see that a laser beam of finite diameter causes a radially directed ponderomotive force in a plasma. This force moves plasma out of the beam, so that ω_p is lower and the dielectric constant ε is higher inside the beam than outside. The plasma then acts as a convex lens, focusing the beam to a smaller diameter.

Problems

8.6 A 1-TW laser beam is focused to a spot 50 μm in diameter on a solid target. A plasma is created and heated by the beam, and it tries to expand. The ponderomotive force of the beam, which acts mainly on the region of critical density ($n = n_c$, or $\omega = \omega_p$), pushes the plasma back and causes "profile modification," which is an abrupt change in density at the critical layer.

(a) How much pressure (in N/m^2 and in lbf/in.^{2}) is exerted by the ponderomotive force? (Hint: Note that F_{NL} is in units of N/m^3 and that the gradient length cancels out. To calculate $\langle \mathrm{E}^2 \rangle$, assume conservatively that it has the same value as in vacuum, and set the 1-TW Poynting flux equal to the beam's energy density times its group velocity in vacuum.)
(b) What is the total force, in tonnes, exerted by the beam on the plasma?
(c) If $T_i = T_e = 1$ keV, how large a density jump can the light pressure support?

8.7 Self-focusing occurs when a cylindrically symmetric laser beam of frequency ω is propagated through an underdense plasma; that is, one which has

$$n < n_c \equiv \varepsilon_0 m\omega^2/e^2$$

In steady state, the beam's intensity profile and the density depression caused by the beam (Fig. 8.12) are related by force balance. Neglecting plasma heating ($KT \equiv KT_e + KT_i = \text{constant}$), prove the relation

$$n = n_0 e^{-\varepsilon_0 \langle E^2 \rangle / 2 n_e KT} \equiv n_0 e^{-\alpha(r)}$$

The quantity $\alpha(0)$ is a measure of the relative importance of ponderomotive pressure to plasma pressure.

8.5 Parametric Instabilities

The most thoroughly investigated of the nonlinear wave–wave interactions are the "parametric instabilities," so called because of an analogy with parametric amplifiers, well-known devices in electrical engineering. A reason for the relatively advanced state of understanding of this subject is that the theory is basically a linear one, but linear about an oscillating equilibrium.

8.5.1 Coupled Oscillators

Consider the mechanical model of Fig. 8.13, in which two oscillators M_1 and M_2 are coupled to a bar resting on a pivot. The pivot P is made to slide back and forth at a frequency ω_0, while the natural frequencies of the oscillators are ω_1 and ω_2. It is clear that, in the absence of friction, the pivot encounters no resistance as long as M_1 and M_2 are not moving. Furthermore, if P is not moving and M_2 is put into motion, M_1 will move; but as long as ω_2 is not the natural frequency of M_1, the amplitude will be small. Suppose now that both P and M_2 are set into motion. The displacement of M_1 is proportional to the product of the displacement of M_2 and the length of the lever arm and, hence, will vary in time as

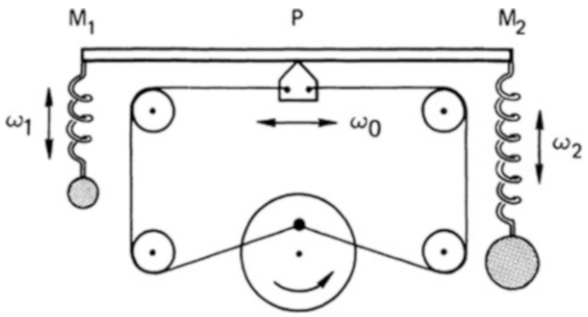

Fig. 8.13 A mechanical analog of a parametric instability

$$\cos\omega_2 t\cos\omega_0 t = \frac{1}{2}\cos\left[(\omega_2+\omega_0)t\right] + \frac{1}{2}\cos\left[(\omega_2-\omega_0)t\right] \tag{8.47}$$

If ω_1 is equal to either $\omega_2+\omega_0$ or $\omega_2-\omega_0$, M_1 will be resonantly excited and will grow to large amplitude. Once M_1 starts oscillating, M_2 will also gain energy, because one of the beat frequencies of ω_1 with ω_0 is just ω_2. Thus, once either oscillator is started, each will be excited by the other, and the system is unstable. The energy, of course, comes from the "pump" P, which encounters resistance once the rod is slanted. If the pump is strong enough, its oscillation amplitude is unaffected by M_1 and M_2; the instability can then be treated by a linear theory. In a plasma, the oscillators P, M_1, and M_2 may be different types of waves.

8.5.2 *Frequency Matching*

The equation of motion for a simple harmonic oscillator x_1 is

$$\frac{d^2x_1}{dt^2} + \omega_1^2 x_1 = 0 \tag{8.48}$$

where ω_1 is its resonant frequency. If it is driven by a time-dependent force which is proportional to the product of the amplitude E_0 of the driver, or pump, and the amplitude x_2 of a second oscillator, the equation of motion becomes

$$\frac{d^2x_1}{dt^2} + \omega_1^2 x_1 = c_1 x_2 E_0 \tag{8.49}$$

where c_1 is a constant indicating the strength of the coupling. A similar equation holds for x_2:

$$\frac{d^2x_2}{dt^2} + \omega_2^2 x_2 = c_2 x_1 E_0 \tag{8.50}$$

Let $x_1 = \overline{x}_1\cos\omega t$, $x_2 = \overline{x}_2\cos\omega' t$, and $E_0 = \overline{E}_0\cos\omega_0 t$. Equation (8.50) becomes

$$\begin{aligned}\left(\omega_2^2 - \omega'^2\right)\overline{x}_2\cos\omega' t &= c_2\overline{E}_0\overline{x}_1\cos\omega_0 t\cos\omega t \\ &= c_2\overline{E}_0\overline{x}_1\frac{1}{2}\{\cos\left[(\omega_0+\omega)t\right] + \cos\left[(\omega_0-\omega)t\right]\}\end{aligned} \tag{8.51}$$

The driving terms on the right can excite oscillators x_2 with frequencies

$$\omega' = \omega_0 \pm \omega \tag{8.52}$$

In the absence of nonlinear interactions, x_2 can only have the frequency ω_2, so we must have $\omega' = \omega_2$. However, the driving terms can cause a frequency shift so that ω' is only approximately equal to ω_2. Furthermore, ω' can be complex, since there is damping (which has been neglected so far for simplicity), or there can be growth (if there is an instability). In either case, x_2 is an oscillator with finite Q and can respond to a range of frequencies about ω_2. If ω is small, one can see from Eq. (8.52) that both choices for ω' may lie within the bandwidth of x_2, and one must allow for the existence of two oscillators, $x_2(\omega_0+\omega)$ and $x_2(\omega_0-\omega)$.

Now let $x_1 = \overline{x}_1 \cos \omega'' t$ and $x_2 = \overline{x}_2 \cos[(\omega_0 \pm \omega)t]$ and insert into Eq. (8.49):

$$\begin{aligned}\left(\omega_1^2 - \omega''^2\right)\overline{x}_1 \cos \omega'' t \\ = c_1 \overline{E}_0 \overline{x}_2 \frac{1}{2}\big(\cos\{[\omega_0 + (\omega_0 \pm \omega)]t\} + \cos\{[\omega_0 - (\omega_0 \pm \omega]t\}\big) \\ = c_1 \overline{E}_0 \overline{x}_2 \frac{1}{2}\{\cos[(2\omega_0 \pm \omega)t] + \cos \omega t\}\end{aligned} \tag{8.53}$$

The driving terms can excite not only the original oscillation $x_1(\omega)$, but also new frequencies $\omega'' = 2\omega_0 \pm \omega$. We shall consider the case $|\omega_0| \gg |\omega_1|$, so that $2\omega_0 \pm \omega$ lies outside the range of frequencies to which x_1 can respond, and $x_1(2\omega_0 \pm \omega)$ can be neglected. We therefore have three oscillators, $x_1(\omega)$, $x_2(\omega_0 - \omega)$, and $x_2(\omega_0 + \omega)$, which are coupled by Eqs. (8.49) and (8.50):

$$\begin{aligned}\left(\omega_1^2 - \omega^2\right)x_1(\omega) - c_1 E_0(\omega_0)[x_2(\omega_0 - \omega) + x_2(\omega_0 + \omega)] = 0 \\ \left[\omega_2^2 - (\omega_0 - \omega)^2\right]x_2(\omega_0 - \omega) - c_2 E_0(\omega_0) x_1(\omega) = 0 \\ \left[\omega_2^2 - (\omega_0 + \omega)^2\right]x_2(\omega_0 + \omega) - c_2 E_0(\omega_0) x_1(\omega) = 0\end{aligned} \tag{8.54}$$

The dispersion relation is given by setting the determinant of the coefficients equal to zero:

$$\begin{vmatrix} \omega^2 - \omega_1^2 & c_1 E_0 & c_1 E_0 \\ c_2 E_0 & (\omega_0 - \omega)^2 - \omega_2^2 & 0 \\ c_2 E_0 & 0 & (\omega_0 + \omega)^2 - \omega_2^2 \end{vmatrix} = 0 \tag{8.55}$$

A solution with $\mathrm{Im}(\omega) > 0$ would indicate an instability.

For small frequency shifts and small damping or growth rates, we can set ω and ω' approximately equal to the undisturbed frequencies ω_1 and ω_2. Equation (8.52) then gives a frequency matching condition:

$$\omega_0 \approx \omega_2 \pm \omega_1 \tag{8.56}$$

When the oscillators are waves in a plasma, ωt must be replaced by $\omega t - \mathbf{k}\cdot\mathbf{r}$. There is then also a wavelength matching condition

$$\mathbf{k}_0 \approx \mathbf{k}_2 \pm \mathbf{k}_1 \tag{8.57}$$

describing spatial beats; that is, the periodicity of points of constructive and destructive interference in space. The two conditions Eqs. (8.56) and (8.57) are easily understood by analogy with quantum mechanics. Multiplying the former by Planck's constant $\hbar$, we have

$$\hbar\omega_0 = \hbar\omega_2 \pm \hbar\omega_1 \tag{8.58}$$

E_0 and x_2 may, for instance, be electromagnetic waves, so that $\hbar\omega_0$ and $\hbar\omega_2$ are the photon energies. The oscillator x_1 may be a Langmuir wave, or plasmon, with energy $\hbar\omega_1$. Equation (8.54) simply states the conservation of energy. Similarly, Eq. (8.53) states the conservation of momentum $\hbar\mathbf{k}$.

For plasma waves, the simultaneous satisfaction of Eqs. (8.52) and (8.53) in one-dimensional problems is possible only for certain combinations of waves. The required relationships are best seen on an ω–k diagram (Fig. 8.14). Figure 8.14a shows the dispersion curves of an electron plasma wave ω_2 (Bohm–Gross wave)

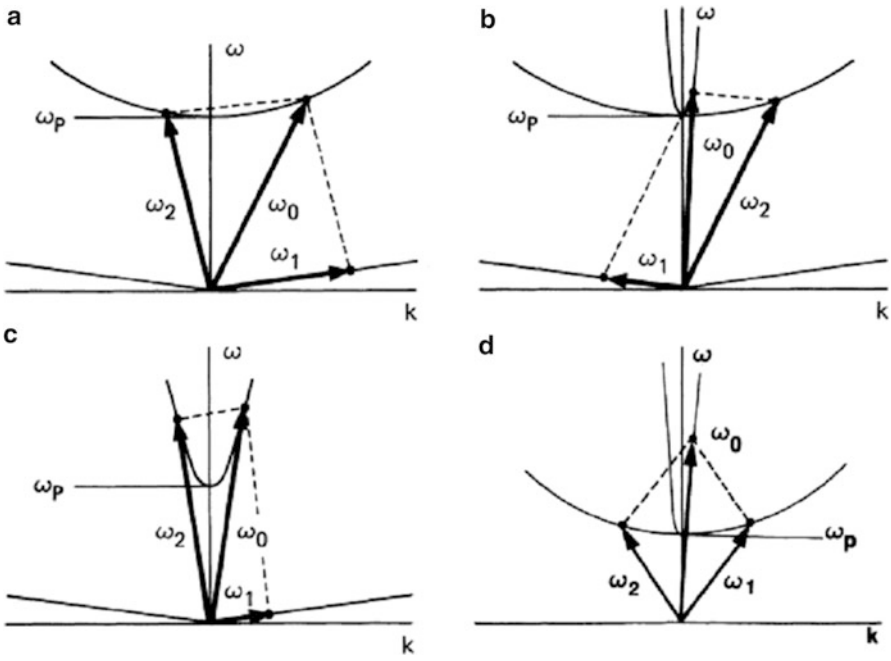

Fig. 8.14 Parallelogram constructions showing the ω- and k-matching conditions for four parametric instabilities: (**a**) electron decay instability, (**b**) parametric decay instability, (**c**) stimulated Brillouin backscattering instability, and (**d**) two-plasmon decay instability. In each case, ω_0 is the incident wave, and ω_1 and ω_2 the decay waves. The *straight lines* are the dispersion relation for ion waves; the *narrow parabolas*, that for light waves; and the *wide parabolas*, that for electron waves

and an ion acoustic wave ω_1 (cf. Fig. 4.13). A large-amplitude electron wave (ω_0, $\mathbf{k}_0$) can decay into a backward moving electron wave (ω_2, $\mathbf{k}_2$) and an ion wave (ω_1, $\mathbf{k}_1$). The parallelogram construction ensures that $\omega_0 = \omega_1 + \omega_2$ and $\mathbf{k}_0 = \mathbf{k}_1 + \mathbf{k}_2$. The positions of ($\omega_0$, $\mathbf{k}_0$) and (ω_2, $\mathbf{k}_2$) on the electron curve must be adjusted so that the difference vector lies on the ion curve. Note that an electron wave cannot decay into two other electron waves, because there is no way to make the difference vector lie on the electron curve.

Figure 8.14b shows the parallelogram construction for the "parametric decay" instability. Here, (ω_0, $\mathbf{k}_0$) is an incident electromagnetic wave of large phase velocity ($\omega_0/k_0 \approx c$). It excites an electron wave and an ion wave moving in opposite directions. Since $|\mathbf{k}_0|$ is small, we have $|\mathbf{k}_1| \approx -|\mathbf{k}_2|$ and $\omega_0 = \omega_1 + \omega_2$ for this instability.

Figure 8.14c shows the ω–k diagram for the "parametric backscattering" instability, in which a light wave excites an ion wave and another light wave moving in the opposite direction. This can also happen when the ion wave is replaced by a plasma wave. By analogy with similar phenomena in solid state physics, these processes are called, respectively, "stimulated Brillouin scattering" and "stimulated Raman scattering."

Figure 8.14d represents the two-plasmon decay instability of an electromagnetic wave. Note that the two decay waves are both electron plasma waves, so that frequency matching can occur only if $\omega_0 \simeq 2\omega_p$. Expressed in terms of density, this condition is equivalent to $n \simeq n_c/4$, when n_c is the critical density (Eq. (4.88)) associated with ω_0. This instability can therefore be expected to occur only near the "quarter-critical" layer of an inhomogeneous plasma.

8.5.3 *Instability Threshold*

Parametric instabilities will occur at any amplitude if there is no damping, but in practice even a small amount of either collisional or Landau damping will prevent the instability unless the pump wave is rather strong. To calculate the threshold, one must introduce the damping rates Γ_1 and Γ_2 of the oscillators x_1 and x_2. Equation (8.48) then becomes

$$\frac{d^2x_1}{dt^2} + \omega_1^2 x_1 + 2\Gamma_1 \frac{dx_1}{dt} = 0 \tag{8.59}$$

For instance, if x_1 is the displacement of a spring damped by friction, the last term represents a force proportional to the velocity. If x_1 is the electron density in a plasma wave damped by electron–neutral collisions, Γ_1 is $\nu_c/2$ (cf. Problem 4.5). Examination of Eqs. (8.49), (8.50), and (8.54) will show that it is all right to use exponential notation and let $d/dt \rightarrow -i\omega$ for x_1 and x_2, as long as we keep E_0 real and allow $\bar{x}_1$ and $\bar{x}_2$ to be complex. Equations (8.49) and (8.50) become

$$\begin{aligned}\left(\omega_1^2-\omega^2-2i\omega\Gamma_1\right)x_1(\omega)&=c_1x_2E_0\\ \left[\omega_2^2-(\omega-\omega_0)^2-2i(\omega-\omega_0)\Gamma_2\right]x_2(\omega-\omega_0)&=c_2x_1E_0\end{aligned}\tag{8.60}$$

We further restrict ourselves to the simple case of two waves—that is, when $\omega\simeq\omega_1$ and $\omega_0-\omega\simeq\omega_2$ but $\omega_0+\omega$ is far enough from ω_2 to be nonresonant—in which case the third row and column of Eq. (8.55) can be ignored. If we now express x_1, x_2, and E_0 in terms of their peak values, as in Eq. (8.53), a factor of 1/2 appears on the right-hand sides of Eq. (8.60). Discarding the nonresonant terms and eliminating $\bar{x}_1$ and $\bar{x}_2$ from Eq. (8.60), we obtain

$$\left(\omega^2-\omega_1^2+2i\omega\Gamma_1\right)\left[(\omega_0-\omega)^2-\omega_2^2-2i(\omega_0-\omega)\Gamma_2\right]=\tfrac{1}{4}c_1c_2\overline{E}_0^2\tag{8.61}$$

At threshold, we may set $\mathrm{Im}(\omega)=0$. The lowest threshold will occur at exact frequency matching; i.e., $\omega=\omega_1$, $\omega_0-\omega=\omega_2$. Then Eq. (8.61) gives

$$c_1c_2\left(\overline{E}_0^2\right)_{\text{thresh}}=16\omega_1\omega_2\Gamma_1\Gamma_2\tag{8.62}$$

The threshold goes to zero with the damping of *either* wave.

Problems

8.8 Prove that stimulated Raman scattering cannot occur at densities above $n_c/4$.

8.9 Stimulated Brillouin scattering is observed when a Nd-glass laser beam ($\lambda=1.06$ μm) irradiates a solid D_2 target ($Z=1$, $M=2M_{\mathrm{H}}$). The backscattered light is red-shifted by 21.9 Å. From x-ray spectra, it is determined that $KT_e=1$ keV. Assuming that the scattering occurs in the region where $\omega_p^2<<\omega^2$, and using Eq. (4.41) with $\gamma_i=3$, make an estimate of the ion temperature.

8.10 For stimulated Brillouin scattering (SBS), we may let x_1 in Eq. (8.60) stand for the ion wave density fluctuation n_1, and x_2 for the reflected wave electric field E_2. The coupling coefficients are then given by

$$\begin{aligned}c_1&=\varepsilon_0k_1^2\omega_p^2/\omega_0\omega_2M\\ c_2&=\omega_p^2\omega_2/n_0\omega_0\end{aligned}$$

and threshold pump intensity in a homogeneous plasma is given by Eq. (8.62). This is commonly expressed in terms of $\langle v_{\mathrm{osc}}^2\rangle$, the rms electron oscillation velocity caused by the pump wave (cf. Eq. (8.37)):

$$v_{\mathrm{osc}}\equiv eE_0/m\omega_0$$

The damping rate Γ_2 can be found from Problem (4.37b) for $\nu/\omega\ll1$.

(a) Show that, for $T_i \ll T_e$ and $v_e^2 \equiv KT_e/m$, the SBS threshold is given by

$$\frac{\langle v_{\text{osc}}^2 \rangle}{v_e^2} = \frac{4\Gamma_1 \nu}{\omega_1 \omega_2}$$

where $\omega_1 = k_1 v_s$ and Γ_1 is the ion Landau damping rate given by Eq. (7.133).

(b) Calculate the threshold laser intensity I_0 in W/cm^2 for SBS of CO_2 (10.6 μm) light in a uniform hydrogen plasma with $T_e = 100$ eV, $T_i = 10$ eV, and $n_0 = 10^{23}$ m^{-3} (Hint: Use the Spitzer resistivity to evaluate ν_{ei}.)

8.11 The growth rate of stimulated Brillouin scattering in a homogeneous plasma far above threshold can be computed from Eq. (8.61) by neglecting the damping terms. Let $\omega = \omega_s + i\gamma$ and assume $\gamma^2 << \omega_s^2$ and $n \ll n_c$. Show that

$$\gamma = \frac{\overline{v}_{\text{osc}}}{2c}\left(\frac{\omega_0}{\omega_s}\right)^{1/2} \Omega_p$$

where $\overline{v}_{\text{osc}}$ is the peak oscillating velocity of the electrons.

8.5.4 Physical Mechanism

The parametric excitation of waves can be understood very simply in terms of the ponderomotive force (Sect. 8.4). As an illustration, consider the case of an electromagnetic wave (ω_0, k_0) driving an electron plasma wave (ω_2, k_2) and a low-frequency ion wave (ω_1, k_1) (Fig. 8.14b). Since ω_1 is small, ω_0 must be close to ω_p. However, the behavior is quite different for $\omega_0 < \omega_p$ than for $\omega_0 > \omega_p$. The former case gives rise to the "oscillating two-stream" instability (which will be treated in detail), and the latter to the "parametric decay" instability.

Suppose there is a density perturbation in the plasma of the form $n_1 \cos k_1 x$; this perturbation can occur spontaneously as one component of the thermal noise. Let the pump wave have an electric field $E_0 \cos \omega_0 t$ in the x direction, as shown in Fig. 8.15. In the absence of a dc field $\mathbf{B}_0$, the pump wave follows the relation $\omega_0^2 = \omega_p^2 + c^2 k_0^2$, so that $k_0 \approx 0$ for $\omega_0 \approx \omega_p$. We may therefore regard E_0 as spatially uniform. If ω_0 is less than ω_p, which is the resonant frequency of the cold electron fluid, the electrons will move in the direction opposite to E_0, while the ions do not move on the time scale of ω_0. The density ripple then causes a charge separation, as shown in Fig. 8.15. The electrostatic charges create a field E_1, which oscillates at the frequency ω_0. The ponderomotive force due to the total field is given by Eq. (8.44):

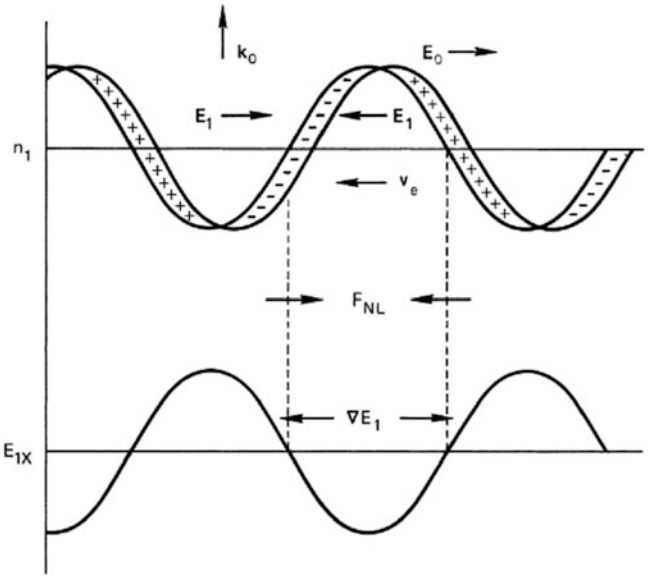

Fig. 8.15 Physical mechanism of the oscillating two-stream instability

$$\mathbf{F}_{\mathrm{NL}} = -\frac{\omega_p^2}{\omega_0^2}\nabla\frac{\left\langle (E_0+E_1)^2\right\rangle}{2}\varepsilon_0 \tag{8.63}$$

Since E_0 is uniform and much larger than E_1, only the cross term is important:

$$\mathbf{F}_{\mathrm{NL}} = -\frac{\omega_p^2}{\omega_0^2}\frac{\partial}{\partial x}\frac{\langle 2E_0E_1\rangle}{2}\varepsilon_0 \tag{8.64}$$

This force does not average to zero, since E_1 changes sign with E_0. As seen in Fig. 8.15, F_{NL} is zero at the peaks and troughs of n_1 but is large where ∇n_1 is large. This spatial distribution causes $\mathbf{F}_{\mathrm{NL}}$ to push electrons from regions of low density to regions of high density. The resulting de electric field drags the ions along also, and the density perturbation grows. The threshold value of F_{NL} is the value just sufficient to overcome the pressure $\nabla n_{i1}(KT_i+KT_e)$, which tends to smooth the density. The density ripple does not propagate, so that $\mathrm{Re}(\omega_1)=0$. This is called the *oscillating two-stream instability* because the sloshing electrons have a time-averaged distribution function which is double-peaked, as in the two-stream instability (Sect. 6.6).

If ω_0 is larger than ω_p, this physical mechanism does not work, because an oscillator driven faster than its resonant frequency moves opposite to the direction of the applied force (this will be explained more clearly in the next section). The directions of $\mathbf{v}_e$, $\mathbf{E}_1$, and $\mathbf{F}_{\mathrm{NL}}$ are then reversed on Fig. 8.15, and the ponderomotive force moves ions from dense regions to less dense regions. If the density

perturbation did not move, it would decay. However, if it were a traveling ion acoustic wave, the inertial delay between the application of the force F_{NL} and the change of ion positions causes the density maxima to move into the regions into which F_{NL} is pushing the ions. This can happen, of course, only if the phase velocity of the ion wave has just the right value. That this value is v_s can be seen from the fact that the phase of the force F_{NL} in Fig. 8.15 (with the arrows reversed now) is exactly the same as the phase of the electrostatic restoring force in an ion wave, where the potential is maximum at the density maximum and vice versa. Consequently, F_{NL} adds to the restoring force and augments the ion wave. The electrons, meanwhile, oscillate with large amplitude if the pump field is near the natural frequency of the electron fluid; namely, $\omega_2^2 = \omega_p^2 + \frac{3}{2}k^2 v_{\mathrm{th}}^2$. The pump cannot have exactly the frequency ω_2 because the beat between ω_0 and ω_2 must be at the ion wave frequency $\omega_1 = kv_s$, so that the expression for F_{NL} in Eq. (8.64) can have the right frequency to excite ion waves. If this frequency matching is satisfied, viz., $\omega_1 = \omega_0 - \omega_2$, both an ion wave and an electron wave are excited at the expense of the pump wave. This is the mechanism of the *parametric decay instability*.

8.5.5 The Oscillating Two-Stream Instability

We shall now actually derive this simplest example of a parametric instability with the help of the physical picture given in the last section. For simplicity, let the temperatures T_i and T_e and the collision rates ν_i and ν_e all vanish. The ion fluid then obeys the low-frequency equations

$$Mn_0 \frac{\partial v_{i1}}{\partial t} = en_0 E = F_{\mathrm{NL}} \tag{8.65}$$

$$\frac{\partial n_{i1}}{\partial t} = n_0 \frac{\partial v_{i1}}{\partial x} = 0 \tag{8.66}$$

Since the equilibrium is assumed to be spatially homogeneous, we may Fourier-analyze in space and replace $\partial/\partial x$ by ik. The last two equations then give

$$\frac{\partial^2 n_{i1}}{\partial t^2} + \frac{ik}{M} F_{\mathrm{NL}} = 0 \tag{8.67}$$

with F_{NL} given by Eq. (8.64). To find E_1, we must consider the motion of the electrons, given by

$$m\left(\frac{\partial v_e}{\partial t} + v_e \frac{\partial}{\partial x} v_e\right) = -e(E_0 + E_1) \tag{8.68}$$

where E_1 is related to the density n_{e1} by Poisson's equation

$$ik\varepsilon_0 E_1 = -en_{e1} \tag{8.69}$$

We must realize at this point that the quantities E_1, v_e, and n_{e1} each has two parts: a high-frequency part, in which the electrons move independently of the ions, and a low-frequency part, in which they move along with the ions in a quasineutral manner. To lowest order, the motion is a high-frequency one in response to the spatially uniform field $\boldsymbol{E}_0$:

$$\frac{\partial v_{e0}}{\partial t} = -\frac{e}{m}E_0 = -\frac{e}{m}\hat{E}_0 \cos\omega_0 t \tag{8.70}$$

Linearizing about this oscillating equilibrium, we have

$$\frac{\partial v_{e1}}{\partial t} + ikv_{e0}v_{e1} = -\frac{e}{m}E_1 = -\frac{e}{m}(E_{1h} + E_{1l}) \tag{8.71}$$

where the subscripts h and l denote the high- and low-frequency parts. The first term consists mostly of the high-frequency velocity v_{eh}, given by

$$\frac{\partial v_{eh}}{\partial t} = -\frac{e}{m}E_{1h} = \frac{n_{eh}e^2}{ik\varepsilon_0 m} \tag{8.72}$$

where we have used Eq. (8.69). The low-frequency part of Eq. (8.71) is

$$ikv_{e0}v_{eh} = -\frac{e}{m}E_{1l}$$

The right-hand side is just the ponderomotive term used in Eq. (8.65) to drive the ion waves. It results from the low-frequency beat between v_{e0} and v_{eh}. The left-hand side can be recognized as related to the electrostatic part of the ponderomotive force expression in Eq. (8.42).

The electron continuity equation is

$$\frac{\partial n_{e1}}{\partial t} + ikv_{e0}n_{e1} + n_0 ikv_{e1} = 0 \tag{8.73}$$

We are interested in the high-frequency part of this equation. In the middle term, only the low-frequency density n_{el} can beat with v_{e0} to give a high-frequency term, if we reject phenomena near $2\omega_0$ and higher harmonics. But $n_{el} = n_{i1}$ by quasineutrality so we have

$$\frac{\partial n_{eh}}{\partial t} + ikn_0 v_{eh} + ikv_{e0}n_{il} = 0 \tag{8.74}$$

Taking the time derivative, neglecting $\partial n_{i1}/\partial t$, and using Eqs. (8.70) and (8.72), we obtain

$$\frac{\partial^2 n_{eh}}{\partial t^2} + \omega_p^2 n_{eh} = \frac{ike}{m} n_{i1} E_0 \tag{8.75}$$

Let n_{eh} vary as exp $(-i\omega t)$:

$$\left(\omega_p^2 - \omega^2\right) n_{eh} = \frac{ike}{m} n_{i1} E_0 \tag{8.76}$$

Equations (8.69) and (8.76) then give the high-frequency field:

$$E_{1h} = -\frac{e^2}{\varepsilon_0 m} \frac{n_{i1} E_0}{\omega_p^2 - \omega^2} \approx -\frac{e^2}{\varepsilon_0 m} \frac{n_{i1} E_0}{\omega_p^2 - \omega_0^2} \tag{8.77}$$

In setting $\omega \approx \omega_0$ we have assumed that the growth rate of n_{i1} is very small compared with the frequency of E_0. The ponderomotive force follows from Eq. (8.64):

$$F_{\mathrm{NL}} \approx \frac{\omega_p^2}{\omega_0^2} \frac{e^2}{m} \frac{ikn_{i1}}{\omega_p^2 - \omega_0^2} \left\langle E_0^2 \right\rangle \tag{8.78}$$

Note that both E_{1h} and F_{NL} change sign with $\omega_p^2 - \omega_0^2$. This is the reason the oscillating two-stream instability mechanism does not work for $\omega_0^2 > \omega_p^2$. The maximum response will occur for $\omega_0^2 \approx \omega_p^2$, and we may neglect the factor (ω_p^2/ω_0^2). Equation (8.67) can then be written

$$\frac{\partial^2 n_{i1}}{\partial t^2} \approx \frac{e^2 k^2}{2Mm} \frac{\hat{E}_0^2 n_{i1}}{\omega_p^2 - \omega_0^2} \tag{8.79}$$

Since the low-frequency perturbation does not propagate in this instability, we can let $n_{i1} = \overline{n}_{i1} \exp \gamma t$, where γ is the growth rate. Thus

$$\gamma^2 \approx \frac{e^2 k^2}{2Mm} \frac{\hat{E}_0^2}{\omega_p^2 - \omega_0^2} \tag{8.80}$$

and γ is real if $\omega_0^2 < \omega_p^2$. The actual value of γ will depend on how small the denominator in Eq. (8.77) can be made without the approximation $\omega^2 \approx \omega_0^2$. If damping is finite, $\omega_p^2 - \omega^2$ will have an imaginary part proportional to $2\Gamma_2 \omega_p$, where Γ_2 is the damping rate of the electron oscillations. Then we have

$$\gamma \propto \hat{E}_0 / \Gamma_2^{1/2} \tag{8.81}$$

Far above threshold, the imaginary part of ω will be dominated by the growth rate γ rather than by Γ_2. One then has

$$\gamma^2 \propto \frac{\hat{E}_0^2}{\gamma} \qquad \gamma \propto \left(\hat{E}_0\right)^{2/3} \tag{8.82}$$

This behavior of γ with E_0 is typical of all parametric instabilities. An exact calculation of γ and of the threshold value of E_0 requires a more careful treatment of the frequency shift $\omega_p - \omega_0$ than we can present here.

To solve the problem exactly, one solves for n_{i1} in Eq. (8.76) and substitutes into Eq. (8.79):

$$\frac{\partial^2 n_{i1}}{\partial t^2} = -\frac{ike}{M} n_{eh} E_0 \tag{8.83}$$

Equations (8.75) and (8.83) then constitute a pair of equations of the form of Eqs. (8.49) and (8.50), and the solution of Eq. (8.55) can be used. The frequency ω_1 vanishes in that case because the ion wave has $\omega_1 = 0$ in the zero-temperature limit.

8.5.6 *The Parametric Decay Instability*

The derivation for $\omega_0 > \omega_p$ follows the same lines as above and leads to the excitation of a plasma wave and an ion wave. We shall omit the algebra, which is somewhat lengthier than for the oscillating two-stream instability, but shall instead describe some experimental observations. The parametric decay instability is well documented, having been observed both in the ionosphere and in the laboratory. The oscillating two-stream instability is not often seen, partly because $\mathrm{Re}(\omega) = 0$ and partly because $\omega_0 < \omega_p$ means that the incident wave is evanescent. Figure 8.16 shows the apparatus of Stenzel and Wong, consisting of a plasma source similar to that of Fig. 8.10, a pair of grids between which the field E_0 is generated by an oscillator, and a probe connected to two frequency spectrum analyzers. Figure 8.17 shows spectra of the signals detected in the plasma. Below threshold, the high-frequency spectrum shows only the pump wave at 400 MHz, while the low-frequency spectrum shows only a small amount of noise. When the pump wave amplitude is increased slightly, an ion wave at 300 kHz appears in the low-frequency spectrum; and at the same time, a sideband at 399.7 MHz appears in the high-frequency spectrum. The latter is an electron plasma wave at the difference frequency. The ion wave then can be observed to beat with the pump wave to give a small signal at the sum frequency, 400.3 MHz.

This instability has also been observed in ionospheric experiments. Figure 8.18 shows the geometry of an ionospheric modification experiment performed with the

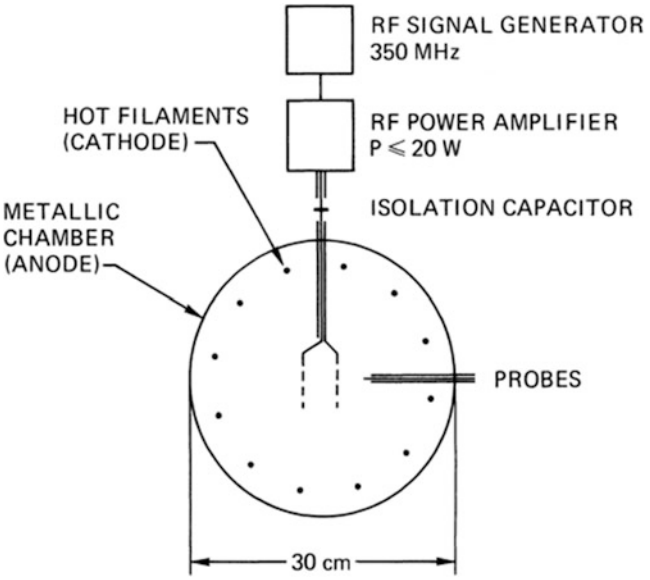

Fig. 8.16 Schematic of an experiment in which the parametric decay instability was verified. [From A. Y. Wong *et al*., *Plasma Physics and Controlled Nuclear Fusion Research*, *1971*, I, 335 (International Atomic Energy Agency, Vienna, 1971).]

large radio telescope at Platteville, Colorado. A 2-MW radiofrequency beam at 7 MHz is launched from the antenna into the ionosphere. At the layer where $\omega_0 \gtrsim \omega_p$, electron and ion waves are generated, and the ionospheric electrons are heated. In another experiment with the large dish antenna at Arecibo, Puerto Rico, the ω and $\mathbf{k}$ of the electron waves were measured by probing with a 430-MHz radar beam and observing the scattering from the grating formed by the electron density perturbations.

Problems

8.12 In laser fusion, a pellet containing thermonuclear fuel is heated by intense laser beams. The parametric decay instability can enhance the heating efficiency by converting laser energy into plasma wave energy, which is then transferred to electrons by Landau damping. If an iodine laser with 1.3-μm wavelength is used, at what plasma density does parametric decay take place?

8.13 (a) Derive the following dispersion relation for an ion acoustic wave in the presence of an externally applied ponderomotive force F_{NL}:

$$\left(\omega^2 + 2i\Gamma\omega - k^2 v_s^2\right) n_1 = ikF_{\mathrm{NL}}/M,$$

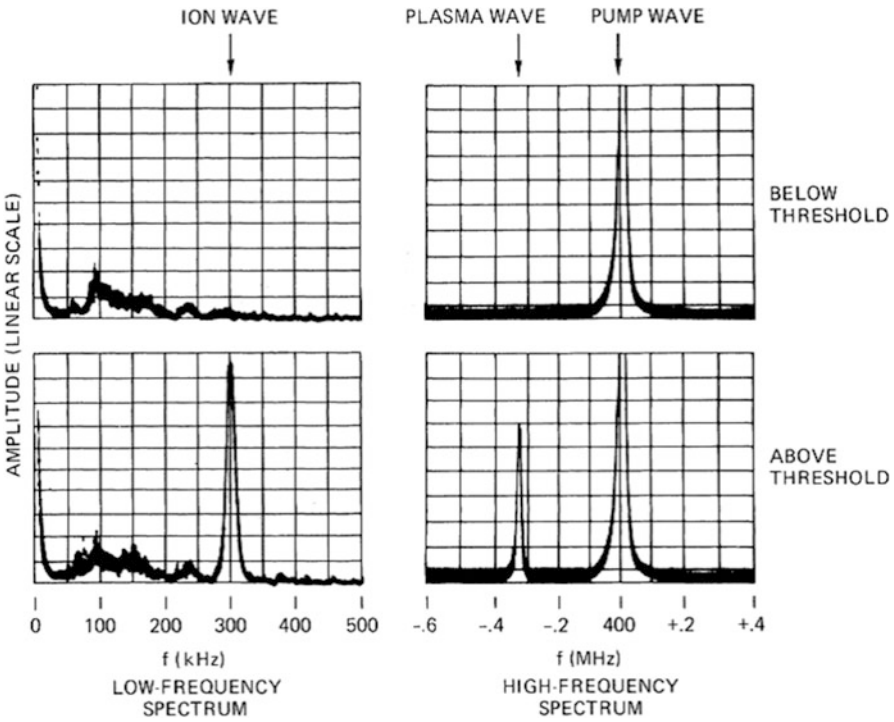

Fig. 8.17 Oscillograms showing the frequency spectra of oscillations observed in the device of Fig. 8.16. When the driving power is just below threshold, only noise is seen in the low-frequency spectrum and only the driver (pump) signal in the high-frequency spectrum. A slight increase in power brings the system above threshold, and the frequencies of a plasma wave and an ion wave simultaneously appear. [Courtesy of R. Stenzel, UCLA.]

where Γ is the damping rate of the undriven wave (when $F_{\mathrm{NL}} = 0$). (Hint: introduce a "collision frequency" ν in the ion equation of motion, evaluate Γ in terms of ν, and eventually replace ν by its Γ-equivalent.)

(b) Evaluate F_{NL} for the case of stimulated Brillouin scattering in terms of the amplitudes E_0 and E_2 of the pump and the backscattered wave, respectively, thus recovering the constant c_1 of Problem (8.10). (Hint: cf. Eq. (8.64).)

8.14 In Fig. 8.17 it is seen that the upper sideband at $\omega_0 + \omega_1$ is missing. Indeed, in most parametric processes the upper sideband is observed to be smaller than the lower sideband. Using simple energy arguments, perhaps with a quantum mechanical analogy, explain why this should be so.

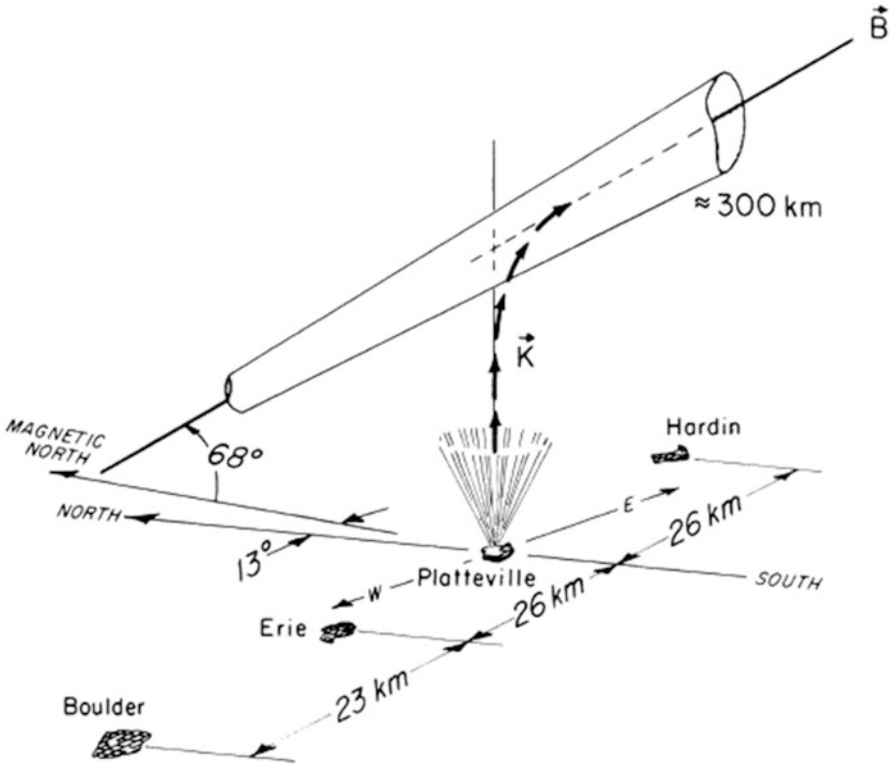

Fig. 8.18 Geometry of an ionospheric modification experiment in which radiofrequency waves were absorbed by parametric decay. [From W. F. Utlaut and R. Cohen, *Science* **174**, 245 (1971).]

8.6 Plasma Echoes

Since Landau damping does not involve collisions or dissipation, it is a reversible process. That this is true is vividly demonstrated by the remarkable phenomenon of plasma echoes. Figure 8.19 shows a schematic of the experimental arrangement. A plasma wave with frequency ω_1 and wavelength λ_1 is generated at the first grid and propagated to the right. The wave is Landau-damped to below the threshold of detectability. A second wave of ω_2 and λ_2 is generated by a second grid a distance l from the first one. The second wave also damps away. If a third grid connected to a receiver tuned to $\omega = \omega_2 - \omega_1$ is moved along the plasma column, it will find an echo at a distance $l' = l\omega_2/(\omega_2 - \omega_1)$. What happens is that the resonant particles causing the first wave to damp out retains information about the wave in their distribution function. If the second grid is made to reverse the change in the resonant particle distribution, a wave can be made to reappear. Clearly, this process can occur only in a very nearly collisionless plasma. In fact, the echo amplitude has been used as a sensitive measure of the collision rate. Figure 8.20 gives a physical picture of why echoes occur. The same basic mechanism lies behind observations

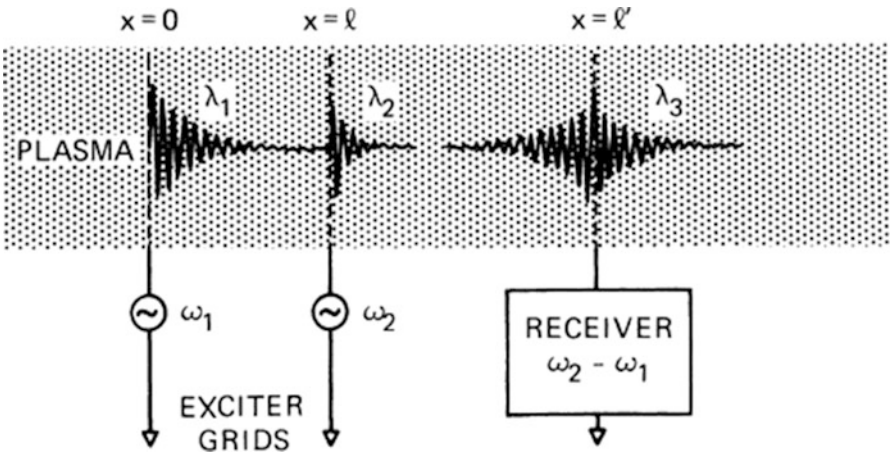

Fig. 8.19 Schematic of a plasma echo experiment. [From A. Y. Wong and D. R. Baker, *Phys. Rev.* **188**, 326 (1969).]

of echoes with electron plasma waves or cyclotron waves. Figure 8.20 is a plot of distance vs. time, so that the trajectory of a particle with a given velocity is a straight line. At $x = 0$, a grid periodically allows bunches of particles with a spread in velocity to pass through. Because of the velocity spread, the bunches mix together, and after a distance l, the density, shown at the right of the diagram, becomes constant in time. A second grid at $x = l$ alternately blocks and passes particles at a higher frequency. This selection of particle trajectories in space–time then causes a bunching of particles to reoccur at $x = l'$.

The relation between l' and l can be obtained from this simplified picture, which neglects the influence of the wave electric field on the particle trajectories. If $f_1(v)$ is the distribution function at the first grid and it is modulated by $\cos \omega_1 t$, the distribution at $x > 0$ will be given by

$$f(x, v, t) = f_1(v) \cos\left(\omega_1 t - \frac{\omega_1}{v} x\right) \tag{8.84}$$

The second grid at $x = l$ will further modulate this distribution by a factor containing ω_2 and the distance $x - l$:

$$f(x, v, t) = f_{12}(v) \cos\left(\omega_1 t - \frac{\omega_1}{v} x\right) \cos\left[\omega_2 t - \frac{\omega_2}{v}(x - l)\right] \tag{8.85}$$

$$\begin{aligned} &= f_{12}(v) \frac{1}{2} \left\{ \cos\left[(\omega_2 + \omega_1)t - \frac{\omega_2(x - l) + \omega_1 x}{v}\right] \right. \\ &\quad \left. + \cos\left[(\omega_2 - \omega_1)t - \frac{\omega_2(x - l) - \omega_1 x}{v}\right] \right\} \end{aligned} \tag{8.86}$$

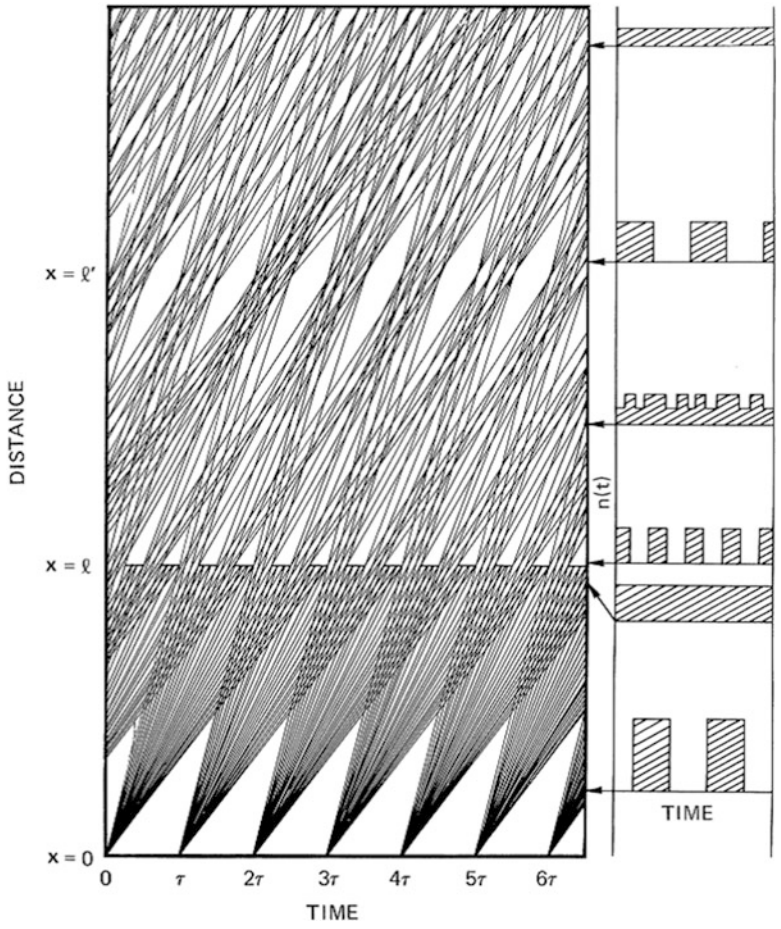

Fig. 8.20 Space–time trajectories of gated particles showing the bunching that causes echoes. The density at various distances is shown at the *right*. [From D. R. Baker, N. R. Ahern, and A. Y. Wong, *Phys. Rev. Lett.* **20**, 318 (1968).]

The echo comes from the second term, which oscillates at $\omega = \omega_2 - \omega_1$ and has an argument independent of v if

$$\omega_2(x - l) = \omega_1 x$$

or

$$x = \omega_2 l/(\omega_2 - \omega_1) \equiv l' \tag{8.87}$$

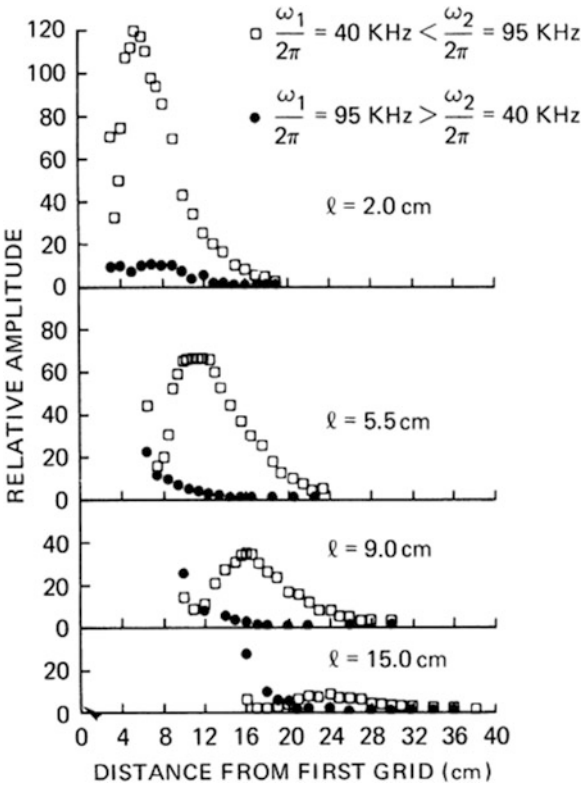

Fig. 8.21 Measurements of echo amplitude profiles for various separations l between the driver grids. The *solid circles* correspond to the case $\omega_2 < \omega_1$, for which no echo is expected. [From Baker, Ahern, and Wong, *loc. cit.*]

The spread in velocities, therefore, does not affect the second term at $x = l'$, and the phase mixing has been undone. When integrated over velocity, this term gives a density fluctuation at $\omega = \omega_2 - \omega_1$. The first term is undetectable because phase mixing has smoothed the density perturbations. It is clear that l' is positive only if $\omega_2 > \omega_1$. The physical reason is that the second grid has less distance in which to unravel the perturbations imparted by the first grid, and hence must operate at a higher frequency.

Figure 8.21 shows the measurements of Baker, Ahern, and Wong on ion wave echoes. The distance l' varies with l in accord with Eq. (8.87). The solid dots, corresponding to the case $\omega_2 < \omega_1$, show the absence of an echo, as expected. The echo amplitude decreases with distance because collisions destroy the coherence of the velocity modulations.

8.7 Nonlinear Landau Damping

When the amplitude of an electron or ion wave excited, say, by a grid is followed in space, it is often found that the decay is not exponential, as predicted by linear theory, if the amplitude is large. Instead, one typically finds that the amplitude

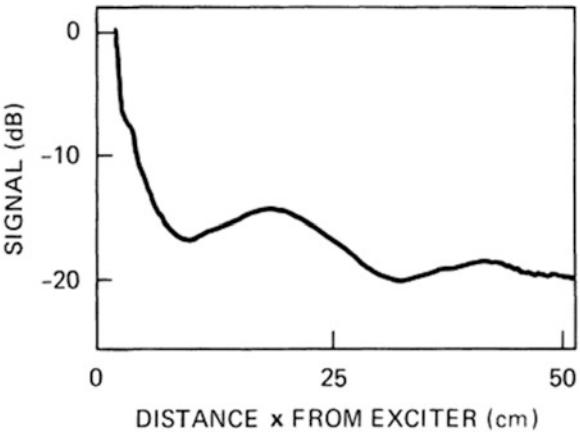

Fig. 8.22 Measurement of the amplitude profile of a nonlinear electron wave showing nonmonotonic decay. [From R. N. Franklin, S. M. Hamberger, H. Ikezi, G. Lampis, and G. J. Smith, *Phys. Rev. Lett.* **28**, 1114 (1972).]

decays, grows again, and then oscillates before settling down to a steady value. Such behavior for an electron wave at 38 MHz is shown in Fig. 8.22. Although other effects may also be operative, these oscillations in *amplitude* are exactly what would be expected from the nonlinear effect of particle trapping discussed in Sect. 7.5. Trapping of a particle of velocity v occurs when its energy in the wave frame is smaller than the wave potential; that is, when

$$|e\phi| > \frac{1}{2}m(v - v_\phi)^2$$

Small waves will trap only these particles moving at high speeds near v_ϕ. To trap a large number of particles in the main part of the distribution (near $v = 0$) would require

$$|q\phi| = \frac{1}{2}\, mv_\phi^2 = \frac{1}{2}m(\omega/k)^2 \tag{8.88}$$

When the wave is this large, its linear behavior can be expected to be greatly modified. Since $|\phi| = |E/k|$, the condition Eq. (8.88) is equivalent to

$$\omega \cong \omega_B, \qquad \text{where} \qquad \omega_B^2 \equiv |qkE/m| \tag{8.89}$$

The quantity ω_B is called the *bounce frequency* because it is the frequency of oscillation of a particle trapped at the bottom of a sinusoidal potential well (Fig. 8.27). The potential is given by

$$\phi = \phi_0(1 - \cos kx) = \phi_0\left(\frac{1}{2}k^2x^2 + \cdots\right) \tag{8.90}$$

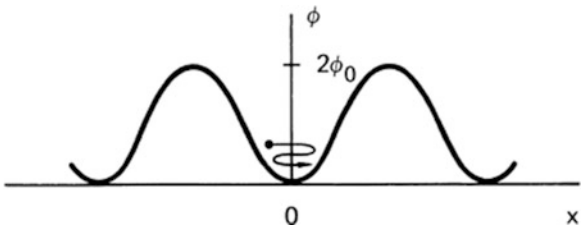

Fig. 8.23 A trapped particle bouncing in the potential well of a wave

The equation of motion is

$$m\frac{d^2x}{dt^2} = -m\omega^2 x = qE = -q\frac{d\phi}{dx} = -qk\phi_0 \sin kx \tag{8.91}$$

The frequency ω is not constant unless x is small, $\sin kx \approx kx$, and ϕ is approximately parabolic. Then ω takes the value ω_B defined in Eq. (8.89). When the resonant particles are reflected by the potential, they give kinetic energy back to the wave, and the amplitude increases. When the particles bounce again from the other side, the energy goes back into the particles, and the wave is damped. Thus, one would expect oscillations in amplitude at the frequency ω_B in the wave frame. In the laboratory frame, the frequency would be $\omega' = \omega_B + kv_\phi$; and the amplitude oscillations would have wave number $k' = \omega'/v_\phi = k[1 + (\omega_B/\omega)]$. The condition $\omega_B \gtrsim \omega$ turns out to define the breakdown of linear theory even when other processes besides particle trapping are responsible.

Another type of nonlinear Landau damping involves the beating of two waves. Suppose there are two high-frequency electron waves (ω_1, k_1) and (ω_2, k_2). These would beat to form an amplitude envelope traveling at a velocity $(\omega_2 - \omega_1)/(k_2 - k_1) \approx d\omega/dk = v_g$. This velocity may be low enough to lie within the ion distribution function. There can then be an energy exchange with the resonant ions. The potential the ions see is the effective potential due to the ponderomotive force (Fig. 8.24), and Landau damping or growth can occur. This damping provides an effective way to heat ions with high-frequency waves, which do not ordinarily interact with ions. If the ion distribution is double-humped, it can excite the electron waves. Such an instability is called a *modulational instability*.

Problems

8.15 Make a graph to show clearly the degree of agreement between the echo data of Fig. 8.21 and Eq. (8.87).

8.16 Calculate the bounce frequency of a deeply trapped electron in a plasma wave with 10-V rms amplitude and 1-cm wavelength (Fig. 8.23).

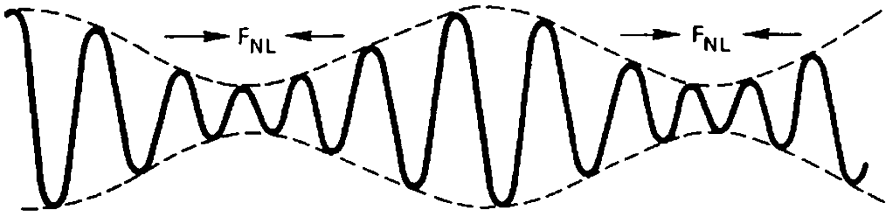

Fig. 8.24 The ponderomotive force caused by the envelope of a modulated wave can trap particles and cause wave-particle resonances at-the group velocity

8.8 Equations of Nonlinear Plasma Physics

There are two nonlinear equations that have been treated extensively in connection with nonlinear plasma waves: The Korteweg–de Vries equation and the nonlinear Schrödinger equation. Each concerns a different type of nonlinearity. When an ion acoustic wave gains large amplitude, the main nonlinear effect is wave steepening, whose physical explanation was given in Sect. 8.3.3. This effect arises from the $\mathbf{v} \cdot \nabla \mathbf{v}$ term in the ion equation of motion and is handled mathematically by the Korteweg–de Vries equation. The wave-train and soliton solutions of Figs. 8.5 and 8.7 are also predicted by this equation.

When an electron plasma wave goes nonlinear, the dominant new effect is that the ponderomotive force of the plasma waves causes the background plasma to move away, causing a local depression in density called a *caviton*. Plasma waves trapped in this cavity then form an isolated structure called an *envelope soliton* or *envelope solitary wave*. Such solutions are described by the nonlinear Schrödinger equation. Considering the difference in both the physical model and the mathematical form of the governing equations, it is surprising that solitons and envelope solitons have almost the same shape.

8.8.1 The Korteweg–de Vries Equation

This equation occurs in many physical situations including that of a weakly nonlinear ion wave:

$$\frac{\partial U}{\partial \tau} + U \frac{\partial U}{\partial \xi} + \frac{1}{2} \frac{\partial^3 U}{\partial \xi^3} = 0 \tag{8.92}$$

where U is amplitude, and τ and ξ are timelike and spacelike variables, respectively. Although several transformations of variables will be necessary before this form is obtained, two physical features can already be seen. The second term in Eq. (8.92) is easily recognized as the convective term $\mathbf{v} \cdot \nabla \mathbf{v}$ leading to wave steepening.

The third term arises from wave dispersion; that is, the k dependence of the phase velocity. For $T_i = 0$, ion waves obey the relation (Eq. (4.48))

$$\omega^2 = k^2 c_s^2 \left(1 + k^2 \lambda_D^2\right)^{-1} \tag{8.93}$$

The dispersive term $k^2\lambda_D^2$ arises from the deviation from exact neutrality. By Taylor-series expansion, one finds

$$\omega = kc_s - \frac{1}{2} k^3 c_s \lambda_D^2 \tag{8.94}$$

showing that the dispersive term is proportional to k^3. This is the reason for the third derivative term in Eq. (8.92). Dispersion must be kept in the theory to prevent very steep wavefronts (corresponding to very large k) from spuriously dominating the nonlinear behavior.

The Korteweg–de Vries equation admits of a solution in the form of a soliton; that is, a single pulse which retains its shape as it propagates with some velocity c (not the velocity of light!). This means that U depends only on the variable $\xi - c\tau$ rather than ξ or τ separately. Defining $\zeta \equiv \xi - c\tau$, so that $\partial/\partial\tau = -c\,d/d\zeta$ and $\partial/\partial\xi = d/d\zeta$, we can write Eq. (8.92) as

$$-c\frac{dU}{d\zeta} + U\frac{dU}{d\zeta} + \frac{1}{2}\frac{d^3U}{d\zeta^3} = 0 \tag{8.95}$$

This can be integrated with the dummy variable ζ':

$$-c\int_\zeta^\infty \frac{dU}{d\zeta'}d\zeta' + \frac{1}{2}\int_\zeta^\infty \frac{dU^2}{d\zeta'}d\zeta' + \frac{1}{2}\int_\zeta^\infty \frac{d}{d\zeta'}\left(\frac{d^2U}{d\zeta'^2}\right)d\zeta' = 0. \tag{8.96}$$

If $U(\zeta)$ and its derivatives vanish at large distances from the soliton ($|\zeta| \to \infty$), the result is

$$cU - \frac{1}{2}U^2 - \frac{1}{2}\frac{d^2U}{d\zeta^2} = 0 \tag{8.97}$$

Multiplying each term by $dU/d\zeta$, we can integrate once more, obtaining

$$\frac{1}{2}cU^2 - \frac{1}{6}U^3 - \frac{1}{4}\left(\frac{dU}{d\zeta}\right)^2 = 0 \tag{8.98}$$

or

$$\left(\frac{dU}{d\zeta}\right)^2 = \frac{2}{3}U^2(3c - U) \tag{8.99}$$

This equation is satisfied by the soliton solution

$$U(\zeta) = 3c\,\mathrm{sech}^2\left[(c/2)^{1/2}\zeta\right] \tag{8.100}$$

as one can verify by direct substitution, making use of the identities

$$\frac{d}{dx}(\mathrm{sech}\,x) = -\mathrm{sech}\,x\,\tanh x \tag{8.101}$$

and

$$\mathrm{sech}^2 x + \tanh^2 x = 1 \tag{8.102}$$

Equation (8.100) describes a structure that looks like Fig. 8.7, reaching a peak at $\zeta = 0$ and vanishing at $\zeta \to \pm\infty$. The soliton has speed c, amplitude $3c$, and half-width $(2/c)^{1/2}$. All are related, so that c specifies the energy of the soliton. The larger the energy, the larger the speed and amplitude, and the narrower the width. The occurrence of solitons depends on the initial conditions. If the initial disturbance has enough energy and the phases are right, a soliton can be generated; otherwise, a large-amplitude wave will appear. If the initial disturbance has the energy of several solitons and the phases are right, an N-soliton solution can be generated. Since the speed of the solitons increases with their size, after a time the solitons will disperse themselves into an ordered array, as shown in Fig. 8.25.

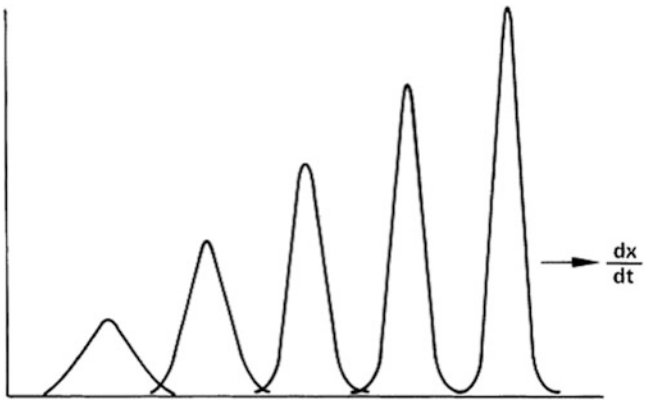

Fig. 8.25 A train of solitons, generated at the *left*, arrayed according to the relation among speed, height, and width

We next wish to show that the Korteweg–de Vries equation describes large-amplitude ion waves. Consider the simple case of one-dimensional waves with cold ions. The fluid equations of motion and continuity are

$$\frac{\partial v_i}{\partial t} + v_i \frac{\partial v_i}{\partial x} = -\frac{e}{m}\frac{\partial \phi}{\partial x} \tag{8.103}$$

$$\frac{\partial n_i}{\partial t} + \frac{\partial}{\partial x}(n_i v_i) = 0 \tag{8.104}$$

Assume Boltzmann electrons (Eq. (3.73)); Poisson's equation is then

$$\varepsilon_0 \frac{\partial^2 \phi}{\partial x^2} = e\left(n_0 e^{e\phi/KT_e} - n_i\right) \tag{8.105}$$

The following dimensionless variables will make all the coefficients unity:

$$\begin{aligned} x' &= x/\lambda_D = x(n_0 e^2/\varepsilon_0 KT_e)^{1/2} \\ t' &= \Omega_p t = t(n_0 e^2/\varepsilon_0 M)^{1/2} \\ \chi &= e\phi/KT_e \qquad n' = n_i/n_0 \\ v' &= v/v_s = v(M/KT_e)^{1/2} \end{aligned} \tag{8.106}$$

Our set of equations becomes

$$\frac{\partial v'}{\partial t'} + v'\frac{\partial v'}{\partial x'} = \frac{\partial \chi}{\partial x'} \tag{8.107}$$

$$\frac{\partial n'}{\partial t'} + \frac{\partial}{\partial x'}\left(n' v'\right) = 0 \tag{8.108}$$

$$\frac{\partial^2 \chi}{\partial x'^2} = e^{\chi} - n' \tag{8.109}$$

If we were to transform to a frame moving with velocity $v' = \mathcal{M}$, we would recover Eq. (8.27). As shown following Eq. (8.27), this set of equations admits of soliton solutions for a range of Mach numbers $\mathcal{M}$.

Problem

8.17 Reduce Eqs. (8.107)–(8.109) to Eq. (8.27) by assuming that χ, n', and v' depend only on the variable $\xi' \equiv x' - \mathcal{M}t'$. Integrate twice as in Eqs. (8.96)–(8.98) to obtain

$$\tfrac{1}{2}\left(d\chi/d\xi'\right)^2 = e^{\chi} - 1 + \mathcal{M}\left[\left(\mathcal{M}^2 - 2\chi\right)^{1/2} - \mathcal{M}\right]$$

Show that soliton solutions can exist only for $1 < \mathcal{M} < 1.6$ and $0 < \chi_{max} < 1.3$.

To recover the *K–dV* equation, we must expand in the wave amplitude and keep one order higher than in the linear theory. Since for solitons the amplitude and speed are related, we can choose the expansion parameter to be the Mach number excess δ, defined to be

$$\delta \equiv \mathcal{M} - 1 \tag{8.110}$$

We thus write

$$\begin{aligned} n' &= 1 + \delta n_1 + \delta^2 n_2 + \cdots \\ \chi' &= \delta\chi_1 + \delta^2\chi_2 + \cdots \\ v' &= \delta v_1 + \delta^2 v_2 + \cdots \end{aligned} \tag{8.111}$$

We must also transform to the scaled variables[1]

$$\xi = \delta^{1/2}\left(x' - t'\right) \qquad \tau = \delta^{3/2}t' \tag{8.112}$$

so that

$$\frac{\partial}{\partial t'} = \delta^{3/2}\frac{\partial}{\partial \tau} - \delta^{1/2}\frac{\partial}{\partial \xi}$$

$$\frac{\partial}{\partial x'} = \delta^{1/2}\frac{\partial}{\partial \xi}$$

Substituting Eqs. (8.111) and (8.113) into Eq. (8.109), we find that the lowest-order terms are proportional to δ, and these give

$$\chi_1 = n_1 \tag{8.114}$$

Doing the same in Eqs. (8.107) and (8.108), we find that the lowest-order terms are proportional to $\delta^{3/2}$, and these give

$$\frac{\partial v_1}{\partial \xi} = \frac{\partial \chi_1}{\partial \xi} = \frac{\partial n_1}{\partial \xi} \tag{8.115}$$

Since all vanish as $\xi \to \infty$, integration gives

$$n_1 = \chi_1 = v_1 \equiv U \tag{8.116}$$

Thus our normalization is such that all the linear perturbations are equal and can be called U. We next collect the terms proportional to δ^2 in Eq. (8.109) and to $\delta^{5/2}$ in Eqs. (8.107) and (8.108). This yields the set

[1] It is not necessary to explain why; the end will justify the means.

$$\frac{\partial^2 \chi_1}{\partial \xi^2} = \chi_2 - n_2 + \frac{1}{2}\chi_1^2 \tag{8.117}$$

$$\frac{\partial v_1}{\partial \tau} - \frac{\partial v_2}{\partial \xi} + v_1 \frac{\partial v_1}{\partial \xi} = -\frac{\partial \chi_2}{\partial \xi} \tag{8.118}$$

$$\frac{\partial n_1}{\partial \tau} - \frac{\partial n_2}{\partial \xi} + \frac{\partial}{\partial \xi}(v_2 + n_1 v_1) \tag{8.119}$$

Solving for n_2 in Eq. (8.117) and for $\partial v_2/\partial \xi$ in Eq. (8.118), we substitute into Eq. (8.119):

$$\frac{\partial n_1}{\partial \tau} + \frac{\partial^3 \chi_1}{\partial \xi^3} - \frac{\partial \chi_2}{\partial \xi} - \frac{1}{2}\frac{\partial \chi_1^2}{\partial \xi} + \frac{\partial v_1}{\partial \tau} + v_1 \frac{\partial v_1}{\partial \xi} + \frac{\partial \chi_2}{\partial \xi} + \frac{\partial}{\partial \xi}(n_1 v_1) = 0 \tag{8.120}$$

Fortunately, χ_2 cancels out, and replacing all first-order quantities by U results in

$$\frac{\partial U}{\partial \tau} + U\frac{\partial U}{\partial \xi} + \frac{1}{2}\frac{\partial^3 U}{\partial \xi^3} = 0 \tag{8.121}$$

which is the same as Eq. (8.92). Thus, ion waves of amplitude one order higher than linear are described by the Korteweg–de Vries equation.

Problem

8.18 A soliton with peak amplitude 12 V is excited in a hydrogen plasma with $KT_e = 10$ eV and $n_0 = 10^{16}$ m^{-3}. Assuming that the Korteweg–de Vries equation describes the soliton, calculate its velocity (in m/s) and its full width at half maximum (in mm). (Hint: First show that the soliton velocity c is equal to unity in the normalized units used to derive the K–dV equation.)

8.8.2 The Nonlinear Schrödinger Equation

This equation has the standard dimensionless form

$$i\frac{\partial \psi}{\partial t} + p\frac{\partial^2 \psi}{\partial x^2} + q|\psi|^2\psi = 0 \tag{8.122}$$

where ψ is the wave amplitude, $i = (-1)^{1/2}$, and p and q are coefficients whose physical significance will be explained shortly. Equation (8.122) differs from the usual Schrödinger equation

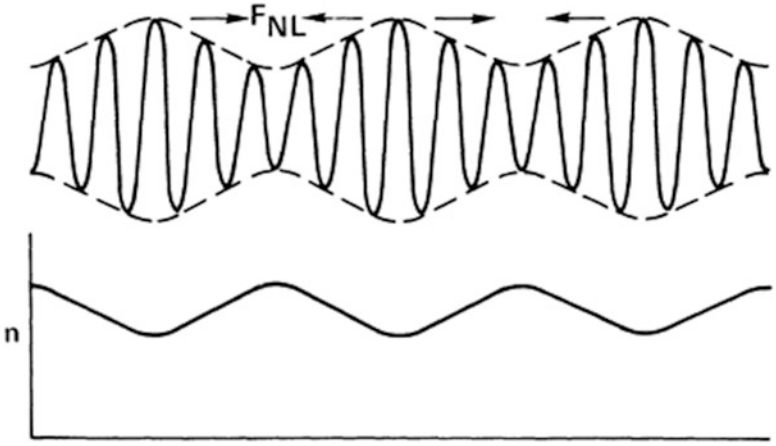

Fig. 8.26 The ponderomotive force of a plasma wave with nonuniform intensity causes ions to flow toward the intensity minima. The resulting density ripple traps waves in its troughs, thus enhancing the modulation of the envelope

$$i\hbar\frac{\partial\psi}{\partial t}+\frac{\hbar^2}{2m}\frac{\partial^2\psi}{\partial x^2}-V(x,t)\psi=0 \tag{8.123}$$

in that the potential $V(x, t)$ depends on ψ itself, making the last term nonlinear. Note, however, that V depends only on the magnitude $|\psi|^2$ and not on the phase of ψ. This is to be expected, as far as electron plasma waves are concerned, because the nonlinearity comes from the ponderomotive force, which depends on the gradient of the wave intensity.

Plane wave solutions of Eq. (8.122) are modulationally unstable if $pq > 0$; that is, a ripple on the envelope of the wave will tend to grow. The picture is the same as that of Fig. 8.24 even though we are considering here fluid, rather than discrete particle, effects. For plasma waves, it is easy to see how the ponderomotive force can cause a modulational instability. Figure 8.26 shows a plasma wave with a rippled envelope. The gradient in wave intensity causes a ponderomotive force which moves both electrons and ions toward the intensity minima, forming a ripple in the plasma density. Plasma waves are trapped in regions of low density because their dispersion relation

$$\omega^2=\omega_p^2+\frac{3}{2}k^2v_{\text{th}}^2 \tag{4.30}$$

permits waves of large k to exist only in regions of small ω_p. The trapping of part of the k spectrum further enhances the wave intensity in the regions where it was already high, thus causing the envelope to develop a growing ripple.

The reason the sign of pq matters is that p and q for plasma waves turn out to be proportional, respectively, to the *group dispersion* dv_g/dk and the *nonlinear frequency shift* $\delta\omega \propto \partial\omega/\partial|\psi|^2$. We shall show later that

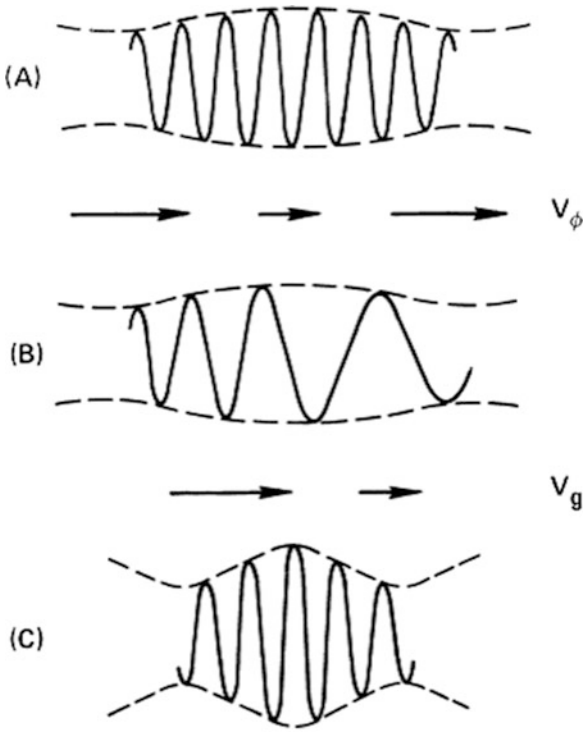

Fig. 8.27 Modulational instability occurs when the nonlinear frequency shift and the group velocity dispersion have opposite signs

$$p = \frac{1}{2}\frac{dv_g}{dk} \qquad q = -\frac{\partial\omega}{\partial|\psi|^2} \propto -\delta\omega \tag{8.123}$$

Modulational instability occurs when $pq > 0$; that is, when $\delta\omega$ and dv_g/dk have opposite signs. Figure 8.27 illustrates why this is so. In Fig. 8.27a, a ripple in the wave envelope has developed as a result of random fluctuations. Suppose $\delta\omega$ is negative. Then the phase velocity ω/k, which is proportional to ω, becomes somewhat smaller in the region of high intensity. This causes the wave crests to pile up on the left of Fig. 8.27b and to spread out on the right. The local value of k is therefore large on the left and small on the right. If dv_g/dk is positive, the group velocity will be larger on the left than the right, so the wave energy will pile up into a smaller space. Thus, the ripple in the envelope will become narrower and larger, as in Fig. 8.27c. If $\delta\omega$ and dv_g/dk were of the same sign, this modulational instability would not happen.

Although plane wave solutions to Eq. (8.123) are modulationally unstable when $pq > 0$, there can be solitary structures called *envelope solitons* which are stable. These are generated from the basic solution

$$w(x,t) = \left(\frac{2A}{q}\right)^{1/2} \operatorname{sech}\left[\left(\frac{A}{p}\right)^{1/2} x\right] e^{iAt} \tag{8.124}$$

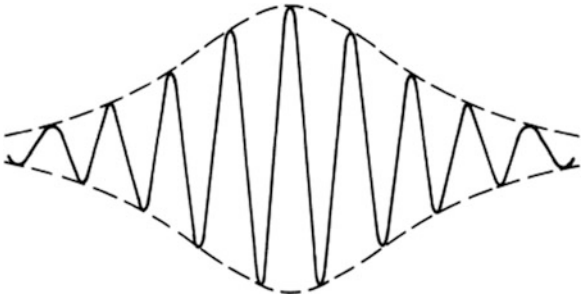

Fig. 8.28 An envelope soliton

where A is an arbitrary constant which ties together the amplitude, width, and frequency of the packet. At any given time, the disturbance resembles a simple soliton (Eq. (8.100)) (though the hyperbolic secant is not squared here), but the exponential factor makes $w(x, t)$ oscillate between positive and negative values. An envelope soliton moving with a velocity V has the more general form (Fig. 8.28)

$$\psi(x,t) = \left(\frac{2A}{q}\right)^{1/2} \operatorname{sech}\left[\left(\frac{A}{p}\right)^{1/2}(x - x_0 - Vt)\right] \exp i\left(At + \frac{V}{2p}x - \frac{V^2}{4p}t + \theta_0\right)\Bigg] \tag{8.125}$$

where x_0 and θ_0 are the initial position and phase. It is seen that the magnitude of V also controls the number of wavelengths inside the envelope at any given time.

Problems

8.19 Show by direct substitution that Eq. (8.124) is a solution of Eq. (8.122).
8.20 Verify Eq. (8.125) by showing that, if $w(x, t)$ is a solution of Eq. (8.122), then

$$\psi = w(x - x_0 - Vt, t)\exp\left[i\left(\frac{V}{2p}x - \frac{V^2}{4p}t + \theta_0\right)\right]$$

is also a solution.

We next wish to show that the nonlinear Schrödinger equation describes large-amplitude electron plasma waves. The procedure is to solve self-consistently for the density cavity that the waves dig by means of their ponderomotive force and for the behavior of the waves in such a cavity. The high-frequency motion of the electrons is governed by Eqs. (4.28), (4.18), and (4.19), which we rewrite respectively in one dimension as

$$\frac{\partial u}{\partial t} = -\frac{e}{m}E - \frac{3KT_e}{mn_0}\frac{\partial n}{\partial x} \tag{8.126}$$

$$\frac{\partial n}{\partial t} + n_0\frac{\partial u}{\partial x} = 0 \tag{8.127}$$

$$\frac{\partial E}{\partial x} = -\varepsilon_0^{-1} en \tag{8.128}$$

where n_0 is the uniform unperturbed density; and E, n, and u are, respectively, the perturbations in electric field, electron density, and fluid velocity. These equations are linearized, so that nonlinearities due to the $\mathbf{u}\cdot\nabla\mathbf{u}$ and $\nabla\cdot(n\mathbf{u})$ terms are not considered. Taking the time derivative of Eq. (8.127) and the x derivative of Eq. (8.126), we can eliminate u and E with the help of Eq. (8.128) to obtain

$$\frac{\partial^2 n}{\partial t^2} - \frac{3KT_e}{m}\frac{\partial^2 n}{\partial x^2} + \frac{n_0 e^2}{m\varepsilon_0} n = 0 \tag{8.129}$$

We now replace n_0 by $n_0 + \delta n$ to describe the density cavity; this is the only nonlinear effect considered. Equation (8.129) is of course followed by any of the linear variables. It will be convenient to write it in terms of u and use the definition of ω_p; thus

$$\frac{\partial^2 u}{\partial t^2} - \frac{3KT_e}{m}\frac{\partial^2 u}{\partial x^2} + \omega_p^2\left(1 + \frac{\delta n}{n_0}\right)u = 0 \tag{8.130}$$

The velocity u consists of a high-frequency part oscillating at ω_0 (essentially the plasma frequency) and a low-frequency part u_l describing the quasineutral motion of electrons following the ions as they move to form the density cavity. Both fast and slow *spatial* variations are included in u_l.

Let

$$u(x,t) = u_l(x,t)e^{-i\omega_0 t} \tag{8.131}$$

Differentiating twice in time, we obtain

$$\frac{\partial^2 u}{\partial t^2} = \left(\ddot{u}_l - 2i\omega_0\dot{u}_l - \omega_0^2 u_l\right)e^{-i\omega_0 t}$$

where the dot stands for a time derivative on the slow time scale. We may therefore neglect $\ddot{u}_l$, which is much smaller than $\omega_0^2 u_l$:

$$\frac{\partial^2 u}{\partial t^2} = -\left(\omega_0^2 u_l + 2i\omega_0\dot{u}_l\right)e^{-i\omega_0 t}$$

Substituting into Eq. (8.130) gives

$$\left[2i\omega_0\dot{u}_l + \frac{3KT_e}{m}\frac{\partial^2 u_l}{\partial x^2} + \left(\omega_0^2 - \omega_p^2 - \omega_p^2\frac{\delta n}{n_0}\right)u_l\right]e^{-i\omega_0 t} = 0 \tag{8.133}$$

We now transform to the dimensionless variables

$$\begin{aligned} t' &= \omega_p t \qquad \omega' = \omega/\omega_p \qquad x' = x/\lambda_D \\ u' &= u(KT_e/m)^{-1/2} \qquad \delta n' = \delta n/n_0 \end{aligned} \tag{8.134}$$

obtaining

$$\left[i\omega_0' \frac{\partial u_l'}{\partial t'} + \frac{3}{2}\frac{\partial^2 u_l'}{\partial x'^2} + \frac{1}{2}\left(\omega_0'^2 - 1 - \delta n'\right) u_l' \right] e^{-i\omega_0' t'} = 0$$

Defining the frequency shift Δ

$$\Delta \equiv \left(\omega_0 - \omega_p\right)/\omega_p = \omega_0' - 1 \tag{8.135}$$

and assuming $\Delta \ll 1$, we have $\omega_0'^2 - 1 \approx 2\Delta$. We may now drop the primes (these being understood), convert back to $u(x, t)$ via Eq. (8.131), and approximate ω_0' by 1 in the first term to obtain

$$i\frac{\partial u}{\partial t} + \frac{3}{2}\frac{\partial^2 u}{\partial x^2} + \left(\Delta - \frac{1}{2}\delta n\right) u = 0 \tag{8.136}$$

Here it is understood that ∂/∂t is the time derivative on the slow time scale, although u contains both the exp $(-i\omega_0 t)$ factor and the slowly varying coefficient u_l. We have essentially derived the nonlinear Schrödinger equation (8.122), but it remains to evaluate δn in terms of $|u_l|^2$.

The low-frequency equation of motion for the electrons is obtained by neglecting the inertia term in Eq. (4.28) and adding a ponderomotive force term from Eq. (8.44)

$$0 = -enE - KT_e \frac{\partial n}{\partial x} - \frac{\omega_p^2}{\omega_0^2}\frac{\partial}{\partial x}\frac{\langle \varepsilon_0 E^2 \rangle}{2}. \tag{8.137}$$

Here we have set $\gamma_e = 1$ since the low-frequency motion should be isothermal rather than adiabatic. We may set

$$\langle E^2 \rangle \cong \frac{m^2\omega_0^2}{e^2}\langle u^2 \rangle \tag{8.138}$$

by solving the high-frequency Eq. (8.126) without the thermal correction. With $E = -\nabla\phi$ and $\chi = e\phi/KT_e$, Eq. (8.137) becomes

$$\frac{\partial}{\partial x}(\chi - \ln n) - \frac{1}{2}\frac{m}{KT_e}\frac{\partial}{\partial x}\langle u^2 \rangle = 0 \tag{8.139}$$

Integrating, setting $n = n_0 + \delta n$, and using the dimensionless units Eq. (8.134), we have

$$\frac{1}{2}\langle u^2 \rangle = \frac{1}{4}|u|^2 = \chi - \ln(1+\delta n) \cong \chi - \delta n \tag{8.140}$$

We must now eliminate χ by solving the cold-ion Eqs. (8.103) and (8.104). Since we are now using the electron variables Eq. (8.134), and since $\Omega_p = \epsilon\omega_p$, $v_s = \epsilon(KT_e/m)^{1/2}$, where $\epsilon \equiv (m/M)^{1/2}$, the dimensionless form of the ion equations is

$$\frac{1}{\epsilon}\frac{\partial u_i}{\partial t} + u_i\frac{\partial u_i}{\partial x} + \frac{\partial \chi}{\partial x} = 0 \tag{8.141}$$

$$\frac{1}{\epsilon}\frac{\partial \delta n_i}{\partial t} + \frac{\partial}{\partial x}[(1+\delta n_i)u_i] = 0 \tag{8.142}$$

Here we have set $n_i' = (n_0 + \delta n_i)/n_0 = 1 + \delta n_i'$ and have dropped the prime. If the soliton is stationary in a frame moving with velocity V, the perturbations depend on x and t only through the combination $\xi = x - x_0 - Vt$. Thus

$$\frac{\partial}{\partial x} = \frac{\partial}{\partial \xi} \qquad \frac{\partial}{\partial t} = -V\frac{\partial}{\partial \xi}$$

and we obtain after linearization

$$-\frac{V}{\epsilon}\frac{\partial u_i}{\partial \xi} + \frac{\partial \chi}{\partial \xi} = 0 \qquad u_i = \frac{\epsilon}{V}\chi \tag{8.143}$$

$$-\frac{V}{\epsilon}\frac{\partial \delta n_i}{\partial \xi} + \frac{\partial u_i}{\partial \xi} = 0 \qquad \delta n_i = \frac{\epsilon}{V}u_i \tag{8.144}$$

From this and the condition of quasineutrality for the slow motions, we obtain

$$\delta n_e = \delta n_i = \frac{\epsilon^2}{V^2}\chi. \tag{8.145}$$

Substituting for χ Eq. (8.140), where δn is really δn_e, we find

$$\delta n_e = \frac{1}{4}|u|^2\left(\frac{V^2}{\epsilon^2} - 1\right)^{-1}. \tag{8.146}$$

Upon inserting this into Eq. (8.136), we finally have

$$i\frac{\partial u}{\partial t} + \frac{3}{2}\frac{\partial^2 u}{\partial x^2} + \left[\Delta - \frac{1}{8}\left(\frac{V^2}{\epsilon^2} - 1\right)^{-1}|u|^2\right]u = 0. \tag{8.147}$$

Comparing with Eq. (8.122), we see that this is the nonlinear Schrödinger equation if Δ can be neglected and

$$p = \frac{3}{2} \qquad q = -\frac{1}{8}\left(\frac{m/M}{V^2 - m/M}\right) \tag{8.148}$$

Finally, it remains to show that p and q are related to the group dispersion and nonlinear frequency shift as stated in Eq. (8.123). This is true for $V^2 \ll m/M$. In dimensionless units, the Bohm–Gross dispersion relation (4.30) reads

$$\omega'^2 = 1 + \delta n' + 3k'^2 \tag{8.149}$$

where $k' = k\lambda_D$, and we have normalized ω to ω_{p0} (the value outside the density cavity). The group velocity is

$$v_g' = \frac{d\omega'}{dk'} = \frac{3k'}{\omega'} \tag{8.150}$$

so that

$$\frac{dv_g'}{dk'} = \frac{3}{\omega'} \cong 3$$

and

$$p = \frac{1}{2}\frac{dv_g'}{dk'} = \frac{3}{2} \tag{8.151}$$

For $V^2 \ll \epsilon^2$, Eq. (8.146) gives

$$\delta n' = -\tfrac{1}{4}|u'|^2$$

so that Eq. (8.144) can be written

$$\omega'^2 = 1 - \tfrac{1}{4}|u'|^2 + 3k'^2 \tag{8.152}$$

Then

$$\begin{aligned} 2\omega' d\omega' &= -\tfrac{1}{4} d|u'|^2 \\ \delta\omega' &\propto \frac{d\omega'}{d|u'|^2} \cong -\frac{1}{8} \end{aligned} \tag{8.153}$$

From Eq. (8.148), we have, for $V^2 \ll \epsilon^2$,

$$q \cong \frac{1}{8} = -\frac{d\omega'}{d|u'|^2}$$

as previously stated.

If the condition $V^2 \ll \epsilon^2$ is not satisfied, the ion dynamics must be treated more carefully; one has coupled electron and ion solitons which evolve together in time. This is the situation normally encountered in experiment and has been treated theoretically.

In summary, a Langmuir-wave soliton is described by Eq. (8.125), with $p = 3/2$ and $q = 1/8$ and with $\psi(x, t)$ signifying the low-frequency part of $u(x, t)$, where u, x, and t are all in dimensionless units. Inserting the exp $(-i\omega_0 t)$ factor and letting x_0 and θ_0 be zero, we can write Eq. (8.125) as follows:

$$u(x,t) = 4A^{1/2}\text{sech}\left[\left(\frac{2A}{3}\right)^{1/2}(x - Vt)\right] \quad \exp\left\{-i\left[\left(\omega_0 + \frac{V^2}{6} - A\right)t - \frac{V}{3}x\right]\right\} \tag{8.154}$$

The envelope of the soliton propagates with a velocity V, which is so far unspecified. To find it accurately involves simultaneously solving a Korteweg–de Vries equation describing the motion of the density cavity, but the underlying physics can be explained much more simply. The electron plasma waves have a group velocity, and V must be near this velocity if the wave energy is to move along with the envelope. In dimensionless units, this velocity is, from Eq. (8.150),

$$V \cong v_g' = \frac{3k'}{\omega'} \cong 3k' \tag{8.155}$$

The term $i(V/3)x$ in the exponent of Eq. (8.154) is therefore just the ikx factor indicating propagation of the waves inside the envelope. Similarly, the factor $-i(V^2/6)t$ is just $-i(3/2)k'^2 t'$, which can be recognized from Eq. (8.149) as the Bohm–Gross frequency for $\delta n' = 0$, the factor ½ coming from expansion of the square root. Since $\omega_0 \simeq \omega_p$, the terms $\omega_0 + (V^2/6)$ represent the Bohm–Gross frequency, and A is therefore the frequency shift (in units of ω_p) due to the cavity in $\delta n'$. The soliton amplitude and width are given in Eq. (8.154) in terms of the shift A, and the high-frequency electric field can be found from Eq. (8.138).

Cavitons have been observed in devices similar to that of Fig. 8.16. Figures 8.29 and 8.30 show two experiments in which structures like the envelope solitons discussed above have been generated by injecting high-power rf into a quiescent plasma. These experiments initiated the interpretation of laser-fusion data in terms of "profile modification," or the change in density profile caused by the ponderomotive force of laser radiation near the critical layer, where $\omega_0 \simeq \omega_p$, ω_0 being the laser frequency.

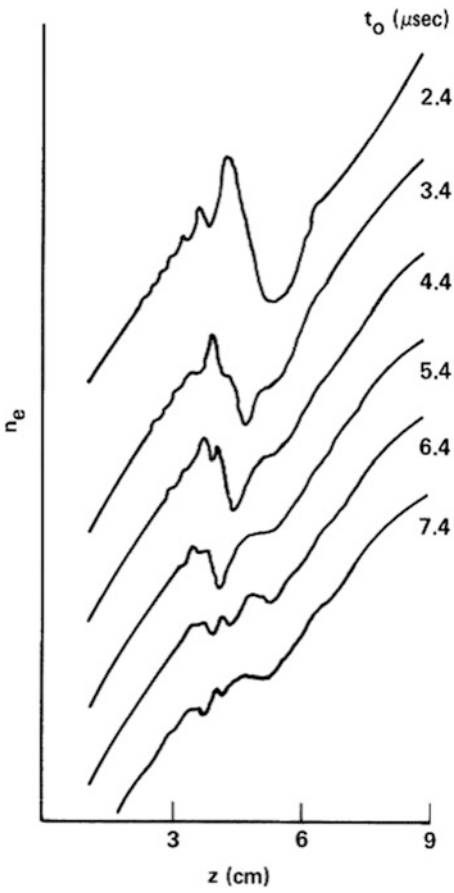

Fig. 8.29 A density cavity, or "caviton," dug by the ponderomotive force of an rf field near the critical layer. The high-frequency oscillations (not shown) were probed with an electron beam. [From H. C. Kim, R. L. Stenzel, and A. Y. Wong, *Phys. Rev. Lett.* **33**, 886 (1974).]

Problems

8.21 Check that the relation between the frequency shift A and the soliton amplitude in Eq. (8.154) is reasonable by calculating the average density depression in the soliton and the corresponding average change in ω_p. (Hint: Use Eq. (8.146) and assume that the sech^2 factor has an average value of $\simeq ½$ over the soliton width.)

8.22 A Langmuir-wave soliton with an envelope amplitude of 3.2 V peak-to-peak is excited in a 2-eV plasma with $n_0 = 10^{15}$ m^{-3}. If the electron waves have $k\lambda_D = 0.3$, find (a) the full width at half maximum of the envelope (in mm), (b) the number of wavelengths within this width, and (c) the frequency shift (in MHz) away from the linear-theory Bohm–Gross frequency.

8.23 A density cavity in the shape of a square well is created in a one-dimensional plasma with $KT_e = 3$ eV. The density outside the cavity is $n_0 = 10^{16}$ m^{-3}, and that inside is $n_i = 0.4 \times 10^{16}$ m^{-3}. If the cavity is long enough that boundary resonances can be ignored, what is the wavelength of the shortest electron plasma wave that can be trapped in the cavity?

8.9 Reconnection

In a collisionless plasma, electrons and ions gyrate around magnetic field lines and are tied to them. If these field lines are brought close together, the plasma will become very dense, and hence highly collisional. In that case, plasma can diffuse across field lines and change the magnetic geometry. Due to kinetic effects, this can happen even without collisions. Reconnection of magnetic field lines occurs in the earth's field on the night side, as shown in Fig. 8.31. The plasma of the solar wind pushes the earth's dipole field away from the sun into a magnetotail, where field lines in opposite directions are brought close to one another. The magnetic configuration can change, as shown in Fig. 8.32. In the magnetotail, the left-hand part becomes a loop connected to the earth's poles, while the right-hand part breaks off to connect to the interplanetary field. At the magnetopause, the lines break and connect to the solar wind.

What happens in the thin reconnecting layer shown in Fig. 8.33 is extremely complicated because both collisional and collisionless damping mechanisms, as well as finite-Larmor-radius effects can occur there. There are many models for the conditions in the layer. In the Sweet-Parker model, B and entrained n diffuse into the layer by resistive diffusion, building up a high density there which must escape at a large velocity v_0 of the order of the Alfvén speed. H. Petschek showed that MHD shocks can occur in fast reconnection, but these do not stay long enough to

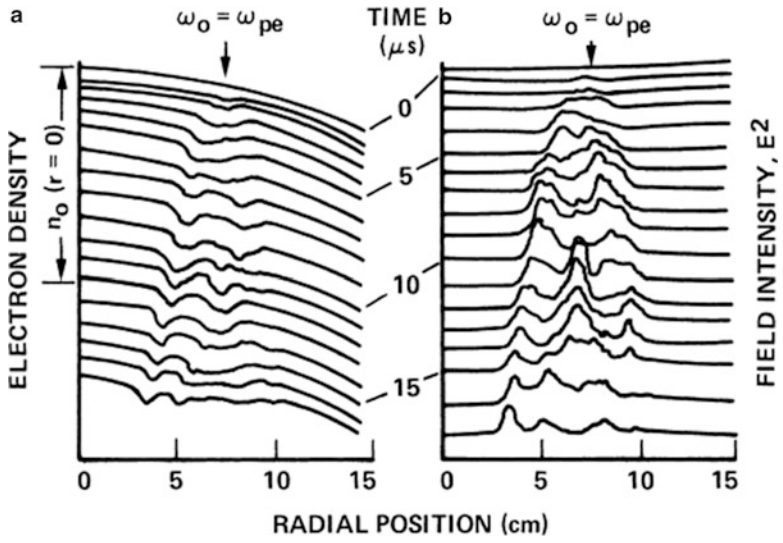

Fig. 8.30 Coupled electron and ion wave solitons. In (**a**) the low-frequency density cavities are seen to propagate to the left. In (**b**) the high-frequency electric field, as measured by wire probes, is found to be large at the local density minima. [From H. Ikezi, K. Nishikawa, H. Hojo, and K. Mima, *Plasma Physics and Controlled Nuclear Fusion Research*, 1974, *II*, 609, International Atomic Energy Agency, Vienna, 1975.]

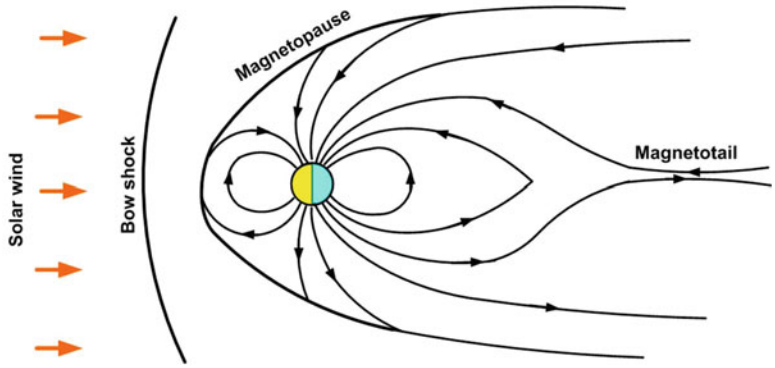

Fig. 8.31 Schematic diagram of the earth's magnetic field, as it is blown by the solar wind into a magnetotail

Fig. 8.32 Reconnection of field lines

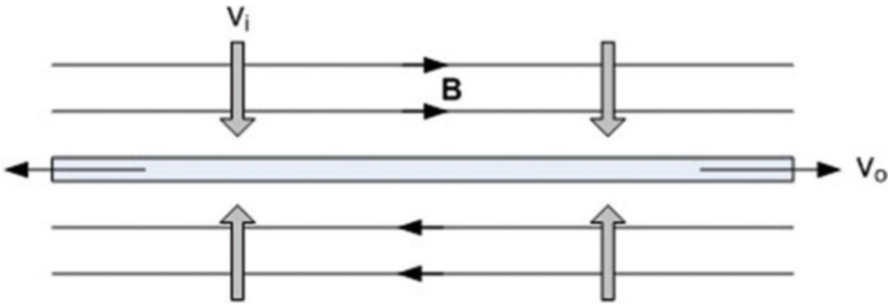

Fig. 8.33 An idealized, thin reconnection layer

have much effect. With the advent of fast computers, W. Daughton has studied three-dimensional reconnection and the generation of turbulence. Reconnection occurs on the surface of the sun itself. These regions manifest themselves as sunspots.

A controlled experiment on reconnection was built at Princeton by M. Yamada and H. Ji, with theoretical support by R. Kulsrud. A diagram of the magnetic field in their machine is shown in Fig. 8.34. The two large rings shown vertically carry current to generate the field lines shown. As the current in the rings is decreased, the

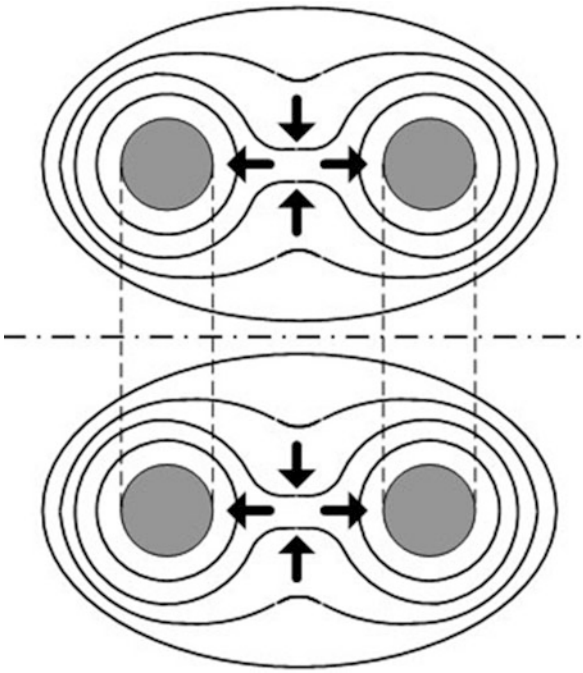

Fig. 8.34 Schematic of the field lines in Yamada's reconnection machine

field lines move in the direction of the arrows, and a reconnection sheet of horizontal cross section forms. If the current is increased, the field lines move opposite to the arrows, and the reconnection sheet has a vertical cross section.

8.10 Turbulence

In Chap. 4 we treated waves in a plasma by linearizing the equations of motion, thus limiting the discussion to waves of small amplitude. Sinusoidal waves cannot grow indefinitely, however; nonlinear effects change their shapes, limit their amplitudes, and ultimately turning them into random turbulence. Figure 8.35 shows a jet of air forming vortices and then breaking into turbulence. In pipes carrying a liquid, the flow is smooth at low velocities, when the velocity has a smooth profile from slow at the edge to fast at the center, as seen in Fig. 8.36 (top). At high velocities, the flow breaks up into turbulence, as in Fig. 8.36 (bottom). The flow slows down, and energy goes into noise. Nonlinearity can happen in a plasma in other ways. For instance, in the plasma oscillation of Fig. 4.2, the amplitude can become so large that the excursion of an electron sheet can overlap the next wavelength. In early experiments in which a current was drawn between an anode and a cathode in a magnetized cylinder, probes inserted into the plasma always detected turbulent fluctuations like those shown in Fig. 8.37. The basic waves that grew into this

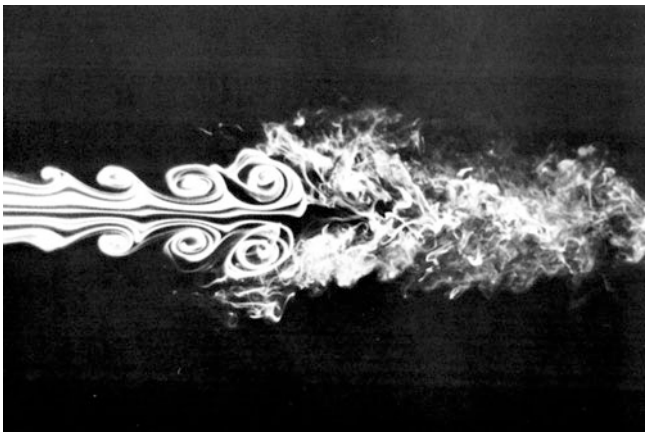

Fig. 8.35 Turbulence in a jet of air, made visible by smoke. [from M. Van Dyke, *An Album of Fluid Motion*, The Parabolic Press, Stanford, CA (1982)]

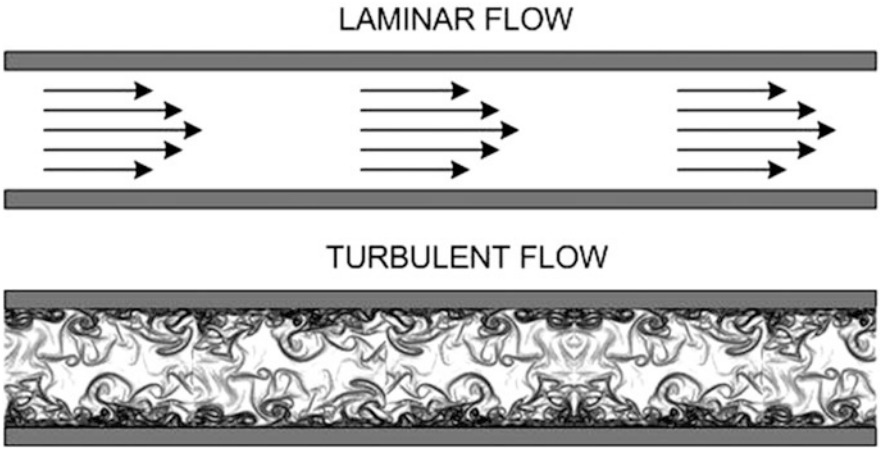

Fig. 8.36 Turbulence in a water pipe

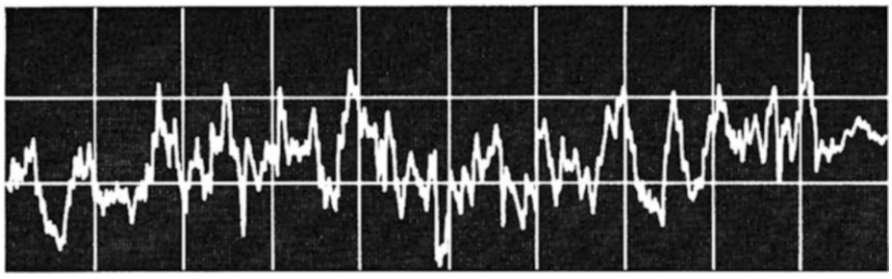

Fig. 8.37 Turbulent potential fluctuations observed in a fusion plasma (Data by the author)

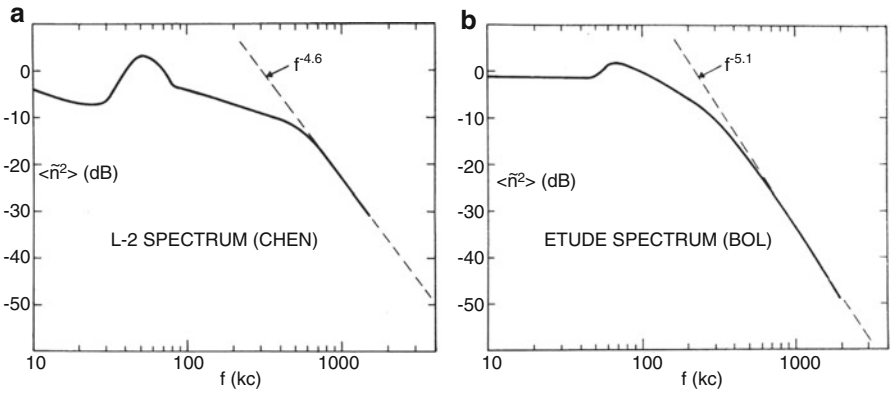

Fig. 8.38 Turbulence spectra in (**a**) the L-2, a reflex arc (2000 G, 10^{12} cm^{-3}); and (**b**) the Etude, a stellarator (6700 G, 10^{13} cm^{-3}). Here, frequency is measured rather than k

nonlinear state were not found for years. We now know of many instabilities that can cause this.

A turbulent field can be decomposed into a spectrum of eddies of different sizes. After excitation, the distribution of sizes—the turbulent spectrum S(k)—will settle down to a form predictable by theory. In two-dimensional systems, such as a sheet of graphene, small eddies will coalesce into larger eddies. In general, however, large eddies will break up into small eddies with a given size distribution. In ordinary hydrodynamics, Kolmogoroff found from dimensional analysis that the spectrum should vary as $k^{-5/3}$. In laboratory plasmas, the turbulence is driven by instabilities such as the Rayleigh-Taylor or drift-wave instabilities, and electron motions are dominated by their $\mathbf{E} \times \mathbf{B}$ drifts. Early experiments at Princeton showed consistent spectra varying as k^{-5} even in entirely different machines, as shown in Fig. 8.38. Because plasma moves very differently from normal fluids, it is not surprising that the exponent of k is quite different. The boundary-dependent peaks in Fig. 8.38 are from the low-frequency instabilities driving the turbulence. By contrast, the spectrum in an early tokamak (PLT) at Princeton, shown in Fig. 8.39, varies as $k^{-2.8}$.

In the modern era, electrostatic probes cannot be inserted into a tokamak, and non-invasive diagnostics must be used, such as reflectometry. The turbulent spectrum will vary greatly with position because of sawtooth oscillations in the interior and Edge Localized Modes near the boundary. Generalizations such as those from the early days can no longer be made. With the advent of fast computers, turbulence in the three-dimensional geometry of a tokamak can be simulated. Figure 8.40 shows such a computation. The magnetic field lines are no longer in the well-ordered magnetic island structure but are completely scrambled.

Basic experiments on plasma turbulence have been done on Walter Gekelman's LAPD (Large Area Plasma Device) machine at the University of California, Los Angeles. Shown in Fig. 8.41 the machine produces a plasma 60 cm in diameter and 17 m long, ionized by electrons emitted from a hot cathode and accelerated through

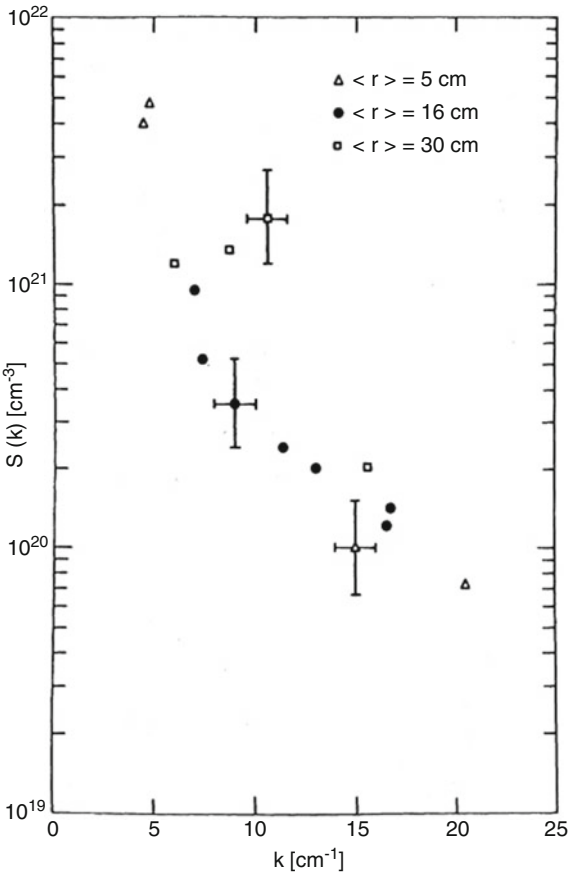

Fig. 8.39 Turbulence spectrum in the PLT tokamak, taken by Mazzucato at three radial positions

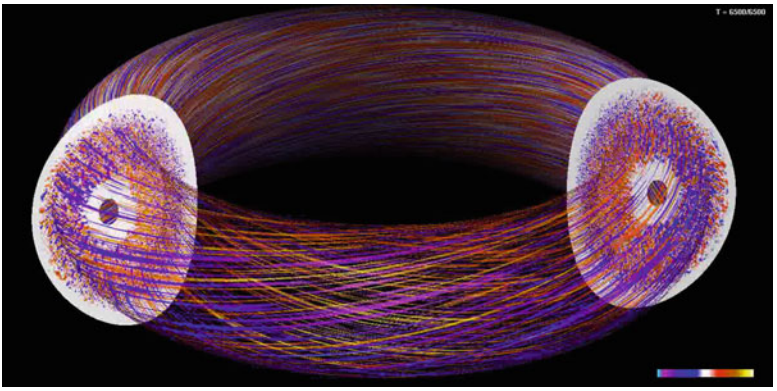

Fig. 8.40 Computer simulation of turbulent field lines in a tokamak. [Courtesy of W.W. Lee, Princeton Plasma Physics Lab]

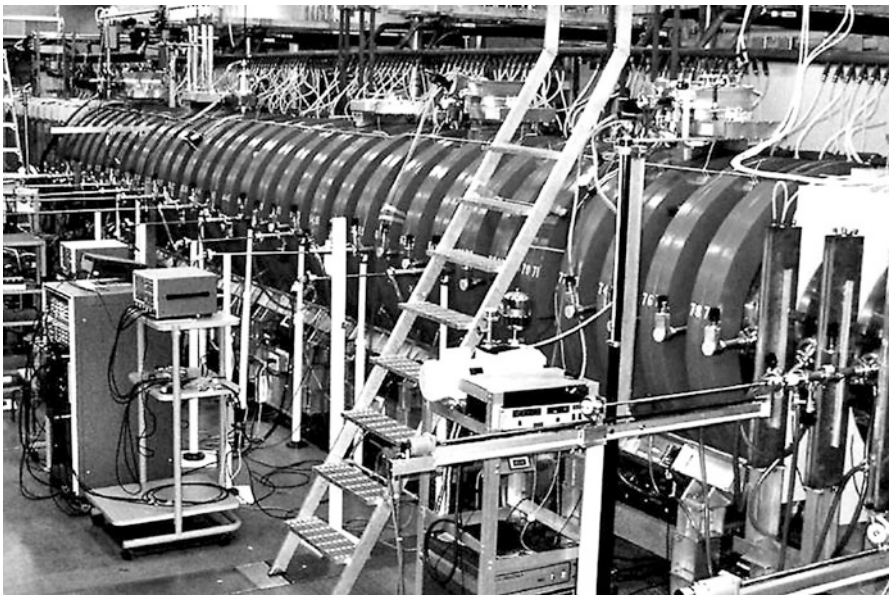

Fig. 8.41 The LAPD machine of W. Gekelman

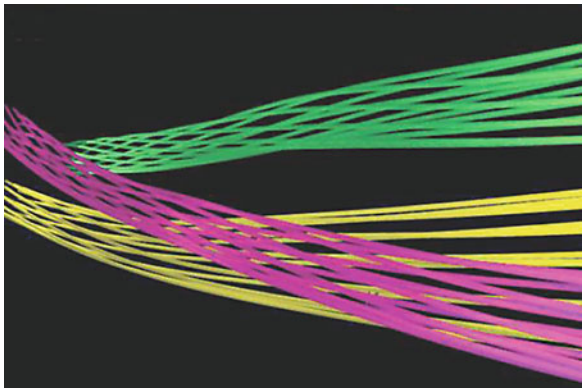

Fig. 8.42 Flux ropes observed in the LAPD machine

a mesh anode. Pulsed for 10–20 ms at 1 Hz, the plasma reaches $n \leq 4 \times 10^{18}$ m^{-3} and $KT_e \leq 8$ eV in $B \leq 0.3$ T (3 kG). The machine is ideally suited for studies of Alfvén waves, which require long length and high B-field.

Fig. 8.42 gives an example of nonlinear effects observed in LAPD which would be hard to predict theoretically. By measuring the currents' B-fields, a current in the plasma was found to filament into curving flux ropes which themselves are composed of smaller filaments.

8.11 Sheath Boundaries

Laboratory plasmas are not infinitely long cylinders, as many theories assume. Plasmas of finite length in a B-field have sheaths at the endplates which control the density profiles. As an example, consider the discharge in Fig. 8.43, which is short enough that gradients in the z direction can be neglected but long enough that the end sheaths do not overlap. The magnetic field is strong enough to confine the electrons to move rapidly only in the z direction, and to move in the r direction only via collisions. But the B-field is weak enough that we can neglect the curvature of the ion orbits inside the radius a. We now describe the *Simon short-circuit effect*, which causes the electrons to behave as if they could cross the magnetic field rapidly although they actually do not.

In Fig. 8.44a, the top of each figure is the radial boundary; the bottom is the interior of the discharge. We assume that radiofrequency power is applied at $r = a$, so that initially n is higher in tube ① than in tube ②. The sheath at the endplate adjusts itself to allow the electron loss to be equal to the ion loss at the Bohm velocity c_s at each r, thus keeping the plasma neutral. The sheath drop $\phi_p(r)$ is therefore given by

$$n\left(\frac{KT_e}{2\pi m}\right)^{1/2} e^{-e\phi_p/KT_e} = n\left(\frac{KT_e}{M}\right)^{1/2} \quad \therefore \quad \frac{e\phi_p}{KT_e} = \ln\left(\frac{M}{2\pi m}\right)^{1/2}, \tag{8.156}$$

where the bracket on the l.h.s. is the random electron velocity in one dimension, and the one on the r.h.s. is the acoustic speed. Since ϕ_p is independent of n, the sheath drop is normally independent of radius. However, when ions are injected at $r = a$, they diffuse inward from tube ① to tube ②. Electrons can't follow them, but the sheath drop on tube ② can increase slightly to trap more electrons to keep tube ② neutral. The sheath on tube ② is becomes thicker than the one on tube ①, as shown in Fig. 8.44a. This mechanism allows electrons to fall into thermal equilibrium and follow the Boltzmann relation for over all radii:

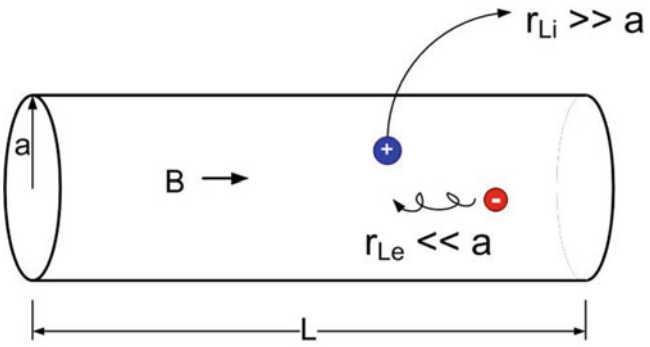

Fig. 8.43 Model of a finite-length laboratory plasma

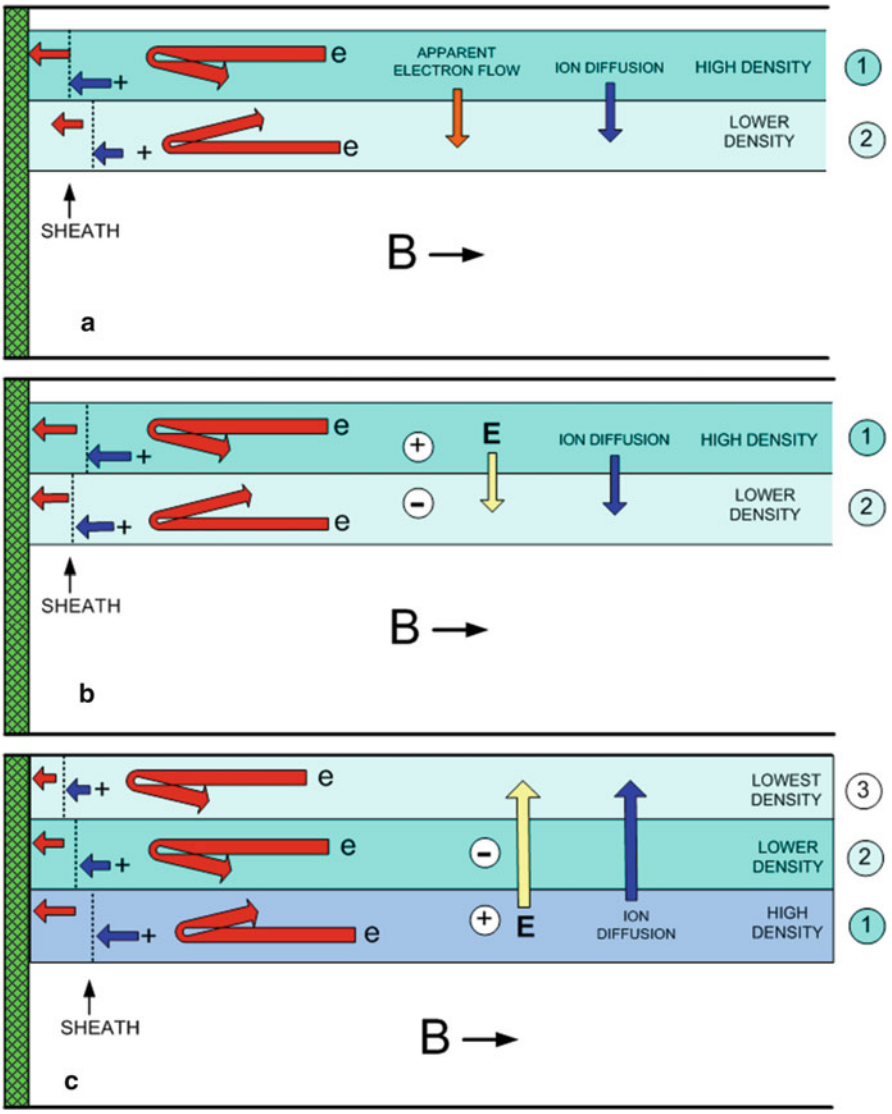

Fig. 8.44 Behavior of sheaths (**a**) initially, (**b**) during approach to equilibrium, and (**c**) in equilibrium

$$n(r) = n_0 e^{e\phi(r)/KT_e(r)}. \tag{3.73}$$

During the approach to equilibrium, the higher density on the outside causes ϕ to be higher there, and this corresponds to a radial E-field pointing inwards, as shown in Fig. 8.44b. The field drives the ions toward the center at a fast rate scaled to KT_e. There cannot be an E-field along **B** because that would cause a large electron

current, and the sheaths have stopped that. Therefore, the ions cannot leave the center except at their low thermal velocities. The ion density builds up there until an outward E-field following Eq. (3.73) drives outward any ions that are created in the interior. If all ions are created at the boundary, $n(r)$ would be flat. The equilibrium sheaths and fields are shown in Fig. 8.44c. A 2011 theory by Curreli and Chen showed that a discharge with the geometry of Fig. 8.43 with sheaths at the endplates will fall into an equilibrium with a "universal" density profile which is independent of pressure and plasma radius a.